Acta Pharmaceutica Sinica B 2022;12(4):1723−1739

Chinese Pharmaceutical Association
Institute of Materia Medica, Chinese Academy of Medical Sciences

Acta Pharmaceutica Sinica B

www.elsevier.com/locate/apsb
www.sciencedirect.com

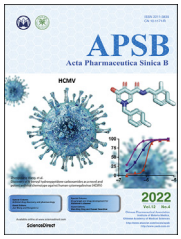

ORIGINAL ARTICLE

High-throughput screening for amyloid-β binding natural small-molecules based on the combinational use of biolayer interferometry and UHPLC−DAD-Q/TOF-MS/MS

Minsong Guo[a,†], Fengdan Zhu[a,†], Wenqiao Qiu[a,c,†], Gan Qiao[a], Betty Yuen-Kwan Law[b], Lu Yu[a], Jianming Wu[a], Yong Tang[a,b], Chonglin Yu[a], Dalian Qin[a,*], Xiaogang Zhou[a,*], Anguo Wu[a,*]

[a]*Sichuan Key Medical Laboratory of New Drug Discovery and Druggability Evaluation, Luzhou Key Laboratory of Activity Screening and Druggability Evaluation for Chinese Materia Medica, School of Pharmacy, Education Ministry Key Laboratory of Medical Electrophysiology, Southwest Medical University, Luzhou 646000, China*
[b]*State Key Laboratory of Quality Research in Chinese Medicine, Macau University of Science and Technology, Taipa, Macau 999078, China*
[c]*Department of Neurosurgery Sichuan Provincial People's Hospital, University of Electronic Science and Technology of China, Chengdu 610000, China*

Received 5 May 2021; received in revised form 11 August 2021; accepted 24 August 2021

KEY WORDS

Alzheimer's disease;
High-throughput screening;
Biolayer interferometry;
UHPLC−DAD-Q/TOF-MS/MS;
Kai-Xin-San

Abstract Discovery of drugs rapidly and effectively is an important aspect for Alzheimer's disease (AD). In this study, a novel high-throughput screening (HTS) method aims at screening the small-molecules with amyloid-β (Aβ) binding affinity from natural medicines, based on the combinational use of biolayer interferometry (BLI) and ultra-high-performance liquid chromatography coupled with diode-array detector and quadrupole/time-of-flight tandem mass spectrometry (UHPLC−DAD-Q/TOF-MS/MS) has been firstly developed. Briefly, the components in natural medicines disassociated from biotinylated Aβ were collected to analyze their potential Aβ binding affinity by UHPLC−DAD-Q/TOF-MS/MS. Here, baicalein was confirmed to exhibit the highest binding affinity with Aβ in *Scutellaria baicalensis*. Moreover, polyporenic acid C (PPAC), dehydrotumulosic acid (DTA), and tumulosic acid (TA) in Kai-Xin-San (KXS) were also identified as potent Aβ inhibitors. Further bioactivity validations indicated that these compounds could inhibit Aβ fibrillation, improve the viability in Aβ-induced PC-12 cells, and

*Corresponding authors. Tel./fax: +86 17769617417.
E-mail addresses: dalianqin@swmu.edu.cn (Dalian Qin), zxg@swmu.edu.cn (Xiaogang Zhou), wuanguo@swmu.edu.cn (Anguo Wu).
†These authors made equal contributions to this work.
Peer review under responsibility of Chinese Pharmaceutical Association and Institute of Materia Medica, Chinese Academy of Medical Sciences.

https://doi.org/10.1016/j.apsb.2021.08.030

decrease the Aβ content and improve the behavioral ability in *Caenorhabditis elegans*. The molecular docking results confirmed that PPAC, DTA, and TA possessed good binding properties with Aβ. Collectively, the present study has provided a novel and effective HTS method for the identification of natural inhibitors on Aβ fibrillation, which may accelerate the process on anti-AD drugs discovery and development.

1. Introduction

Alzheimer's disease (AD), an age-related neurodegenerative disease, has become the most common dementia and accounted for almost 60%−80% of all cases[1]. The epidemiological data indicated that the prevalence of AD is increasing with the world's population ageing. Currently, there are approximately 35.6 million AD patients worldwide[2,3]. The clinical symptoms of AD manifest mainly as progressive memory loss, cognitive dysfunction, distraction, mood disorder, and personality change[4]. At present, AD is still an irreversible and incurable neurodegenerative disease. The mechanistic studies indicated that the pathology of AD is closely related the occurrence of neuroinflammation and neuronal death induced by the increasingly accumulated misfolded protein aggregates, such as β-amyloid (Aβ) and Tau[5]. Among them, Aβ is generated from amyloid precursor protein (APP) through the sequential cleavage of β- and γ-secretase[6]. The generated fragments including $A\beta_{1-40}$ and $A\beta_{1-42}$ aggregates are recognized to be the most toxic types, which are accumulated extracellularly to form Aβ fibrils and ultimately form senile plaque in the brain of AD patients[7]. In the early state of AD, Aβ can still be cleared through the autophagy–lysosome pathway (ALP)[8] and the ubiquitin−proteasome pathway (UPP) in neurons or engulfed by microglia[9]. However, both ALP and UPP are dysregulated with age, and the clearance of Aβ cannot be executed effectively[10]. Therefore, targeting inhibition of Aβ fibrils generation has become a promising therapeutic strategy for AD.

It has been proved for a long time that natural medicines such as traditional Chinese medicines (TCMs) are safe and exhibit the favorable characteristics, including multi-components, multi-efficacies, and multi-targets[11]. In addition, natural medicines have rich resources for the discovery of new drugs[12]. Many natural medicines or their ingredients were found to exhibit potent neuroprotective effects in multiple models of AD[13−17]. For example, *Aegle marmelos* extract[18], lychee seed fraction[19], *Cirsium japonicum* var. maackii extract[20], curcumin, ferulic acid[21], quercetin[13], chlorogenic acid[22], and polysaccharides in *Lycium barbarum*[23] were reported to inhibit Aβ-induced cytotoxicity and ameliorate the Aβ pathology in AD animals. However, there are still very few promising compounds identified from natural medicines for the treatment of AD. This may be due to the discovery of bioactive components from natural medicines such as Chinese medical herbs or formulas with complex chemical constituents is time-consuming and laborious[24]. Therefore, it is very important to develop an effective, time-saving, and reliable method for the screening of small-molecule inhibitors of Aβ from natural medicines. To date, several screening methods reported, including cell membrane chromatography (CMC)[25], network pharmacology and molecular docking[26], affinity ultrafiltration with drug targets of interest coupled to high-performance liquid chromatography−mass spectrometry (AUF−HPLC−MS/MS)[27], bubble-generating magnetic liposomes coupled with liquid chromatography−mass spectrometry (LC−MS)[28], etc. In general, most of them are developed based the application of advanced analytical instruments, such as HPLC, MS, and nuclear magnetic resonance (NMR)[29,30].

In our previous studies, we employed CMC, target-fishing approach, and protein-molecule interaction coupled with ultra-HPLC coupled with diode-array detector and time of flight/mass spectrometry (UHPLC−DAD-TOF/MS) to identify the bioactive components from Chinese medical herbs[31]. Here, we developed a more rapid and reliable high-throughput screening (HTS) method for the discovery of inhibitors of Aβ fibrillation from TCMs by the combinational use of biolayer interferometry (BLI) technology and UHPLC−DAD and quadrupole with a time of flight tandem mass spectrometry (UHPLC−DAD-Q/TOF-MS/MS). *Scutellaria baicalensis* (SB) is widely reported to inhibit Aβ both *in vitro* and *in vivo*[32]. In addition, we previously identified that baicalein and baicalin exhibited binding affinity with Aβ[31]. Therefore, SB was further selected to validate the feasibility of the present screening method. Similarly, baicalein and baicalin were the components in SB that showed the best binding characteristics with Aβ[31]. Moreover, we further employed this method to identify the Aβ fibrilization inhibitor from Kai-Xin-San (KXS), a classical Chinese medical formula composed of Ginseng Radix, Polygalae Radix, Acori Tatarinowii Rhizoma, and Poria. KXS is commonly used for the treatment of dementia in ancient China and also in modern Chinese medicine hospitals[33]. Finally, three compounds in Poria, including polyporenic acid C (PPAC), dehydrotumulosic acid (DTA), and tumulosic acid (TA), were identified. The bioassay results showed that PPAC, DTA, and TA significantly inhibited Aβ fibrils formation, improved the viability of $A\beta_{1-42}$-treated PC-12 cells, as well as decreased the Aβ content and improved behavioral abilities in *Caenorhabditis elegans* of AD. The molecular docking results indicated that PPAC, DTA, and TA possessed good binding property with Aβ. Collectively, the current study presents a novel and effective HTS method for the natural inhibitors of Aβ fibrillation from TCMs based on the combinational use of BLI and UHPLC−DAD-Q/TOF-MS/MS, which accelerates the discovery and development of anti-AD drugs in the future.

2. Materials and methods

2.1. Chemicals and reagents

3-(4,5-Dimethyl-thiazol-2-yl)-2,5-dimethyl-tetrazolium bromide (MTT, M2128) and Thioflavin T (ThT, 596200) were acquired from Sigma−Aldrich (St. Louis, USA). Water used for experiment was prepared using the Milli-Q integral system (Millipore, Billerica, MA, USA). Acetonitrile reagent was bought from Anaqua

Chemicals Supply (ACS, Houston, TX, USA). $A\beta_{1-42}$ peptide was from China Peptides Co., Ltd. (Shanghai, China). EZ-Link NHS-LC-LC-Biotin was purchased from Thermo Fisher Scientific Inc., (Waltham, MA, USA). Streptavindin (SA) biosensors used for BLI analysis were obtained from PALL ForteBio (NY, USA). Hoechst 33342 (B2261) and propidium iodide (PI, P4170) were bought from Sigma (St. Louis, MO, USA). The Annexin V-FITC/PE Apoptosis Detection Kit was purchased from BD Biosciences (San Jose, CA, USA). The antibodies including 6E10 (803001; BioLegend), A11 (AHB0052; Invitrogen), and OC (ab201062; Abcam) were used in this study. Ponceau S was purchased from Saint-Bio (Shanghai, China).

2.2. Cell culture

PC-12 cells were purchased from American Type Culture Collection (ATCC; Rockville, MD, USA) and maintained in Dulbecco's modified Eagle's medium (DMEM) culture medium which was supplemented with 10% horse serum (HS), 5% fetal bovine serum (FBS), and 1% penicillin/streptomycin (PS). PC-12 cells used for the *in vitro* experiments were cultured in an incubator with 5% humidified CO_2 and 37 °C.

2.3. Extract preparation of natural medicines

Chinese medical herbs including Scutellaria Radix and Poria, as well as the Chinese medical formula KXS composed of Ginseng Radix, Polygalae Radix, Acori Tatarinowii Rhizoma, and Poria were weighed and crushed, respectively. Then, the crude powders were extracted by reflux method using 10 times of its volume of water at boiling temperature for 1 h. After 3 repeat extractions, the water extract solutions were combined, filtered, and concentrated. The dried extract was quantified and dissolved by DMSO to the stock concentration of 200 mg/mL. All the extracts were stored at −80 °C until further experiments.

2.4. Preparation of $A\beta_{1-42}$ peptide

$A\beta_{1-42}$ peptide was prepared as described previously[31]. To begin with, $A\beta_{1-42}$ peptide (5 mg) was dissolved with appropriate volume of hexafluoroisopropanol (HFIP, Sigma) solution. The HFIP solution was then aliquoted and dried under the nitrogen flow. The generated thin $A\beta_{1-42}$ peptide film was then stored at −80 °C until further BLI analysis, Western blot analysis, and the evaluation of cell viability experiments.

2.5. Isolations of PPAC, DTA, and TA

The crude powder of Poria was extracted by ethyl acetate reagent to obtain the extract for the isolation of PPAC, DTA, and TA. In brief, 100 g of Poria dry extract was loaded onto the open glass column filled with silica gel particles. The components in Poria ethyl acetate extract were eluted by the reagent system consisting of methanol and dichloromethane. Then, the components were collected for the further purification on a reversed-phase YMC-Triart C18 column (250 mm × 10 mm, S-5 μm, 12 nm, YMC Co., Ltd. Kyoto, Japan) which was equipped on a Shimadzu (Kyoto, Japan) Prominence HPLC system. This HPLC system consists of two LC-20AD pumps, a SIL-20ACHT autosampler, a CBM-20A communications bus module, an SPD-M20A diode array detector, and a CTO-20AC column heater-cooler. The column temperature was maintained at 30 °C. The mobile phase was composed of methanol and 0.1% formic acid in water (80:20, *v*/*v*), and the flow rate was set at 4 mL/min. Three main peaks corresponding to PPAC, DTA, and TA were collected. Then, the collected solution was evaporated by the rotary vacuum concentration instrument.

2.6. BLI analysis

The preparation of biotinylated $A\beta_{1-42}$ and the BLI analysis were performed according to the reported literatures[34,35]. In brief, the above generated $A\beta_{1-42}$ peptide film was dissolved in PBS to make a concentration of 25 μg/mL, which was subjected to the biotinylation with EZ-Link NHS-LC-LC-Biotin. After pre-wetting the SA biosensor with PBS to record the baseline, the biotinylated $A\beta_{1-42}$ in 96-well black F-bottom plates (655209, Greiner, Germany) were directly immobilized on the SA biosensor. The extract of natural medicines or single compounds were diluted by PBS (containing 15% DMSO and 0.02% Tween 20) to the appropriate concentrations with the final volume of 200 μL per well. At the same time, an equal volume of PBS (containing 15% DMSO and 0.02% Tween 20) was added to wells and set as the control group. A total of 4 major steps, including loading for 300 s, baseline for 60 s, association for 120 s, and dissociation for 120 s, are repeated circularly. The data were acquired and analyzed by ForteBio Octet® Data Acquisition and Data Analysis software (Port Washington, NY, USA).

2.7. UHPLC−DAD-Q/TOF-MS/MS conditions

Analyses of all samples were performed on a UHPLC system (Shimadzu, Kyoto, Japan) which is composed of a solvent delivery system LC-3AD, an autosampler SIL30ACXR, a column oven CTO-30AC, a degasser DGU-20A3, and a controller CBM-20A. The separation was conducted on an UHPLC Agilent column Zorbax EcLipse Plus C18 at a flow rate of 0.3 mL/min (1.8 μm, 100 mm × 2.1 mm). During the analysis, the column temperature was maintained at 40 °C. The mobile phase is made of water with 0.1% formic acid (A) and acetonitrile with 0.1% formic acid (B). The elution program was set as follows: 0−15 min, 10%−95% B; 15.01−19 min, 10% B. A triple TOFM X500R system equipped with a Duo Spray source (AB SCIEX, Foster City, CA, USA) was used to conduct the MS analysis in the negative electrospray ion mode. The parameters of electrospray ionization (ESI) were set as follows: ion spray voltage: −4500 V; curtain gas: 35 psi; ion source temperature: 550 °C; declustering potential (DP): −100 V, nebulizer gas (GS 1): 55 psi, and heater gas (GS 2): 55 psi. *m*/*z* 100−1600 Da was used for the MS scan. Data analysis were performed by the Peak View® 1.4 software (AB SCIEX Foster City, CA, USA).

2.8. Calculation of the relative binding amount

Calculation of the relative binding amount (RBA) of the compounds with Aβ in TCMs was performed according to the following procedures. In brief, after BLI analysis, the samples, including the dissociation buffer without extract of natural medicines (S1), the dissociation buffer with extract of natural

medicines (S2), and the extract of natural medicines used for the BLI assay (S3), were collected for the analysis by the UHPLC−DAD-Q/TOF-MS/MS instrument. Through comparison of the identified compounds in the above samples, the compounds that could be detected in S2 and S3 but cannot be detected in S1 were recognized to be the potential compounds with Aβ binding affinity. Then, the relative binding amount (RBA) of compounds was calculated using Eq.(1):

$$\text{RBA}\ (\%) = (\text{Peak area of the compounds in S2} / \text{Peak area of the compounds in S3}) \times 100 \quad (1)$$

2.9. MTT assay

100 μL of PC-12 cells were seeded into 96-well plate with a density of 30,000 cells/mL. On the second day, PC-12 cells were treated with the test drugs in the absence or presence of Aβ_{1-42} for 24 h. After treatment, 10 μL of MTT solution (5 mg/mL) was added to the wells, which was followed by an incubation at 37 °C for 4 h. Then, the solution was discarded and the blue formazan was dissolved by 100 μL of DMSO. The optical density (OD) value of the solution was read by a microplate spectrophotometer (BioTek, VT Lab, USA) with a wavelength of 570 nm. The cell viability was calculated according to Eq.(2):

$$\text{Cell viability}\ (\%) = \left[\text{OD}_{\text{experimental}} - \text{OD}_{\text{blank}}\right] / \left[\text{OD}_{\text{control}} - \text{OD}_{\text{blank}}\right] \times 100 \quad (2)$$

2.10. ThT assay

2 μL of freshly prepared 1 mmol/L of Aβ_{1-42} was mixed with PBS in the presence or absence of the test drugs including PPAC, DTA, TA, curcumin (Cur), Poria or KXS extract. The final volume of above solutions was set to 100 μL[36]. At the incubation time points of 0, 24, and 48 h, 50 μL of ThT (20 μmol/L) was diluted with PBS (pH = 7.4) and mixed with 100 μL of the above solutions. Then, the mixture solutions were transferred into black 96-well plates for the reading of OD values by a microplate spectrophotometer (BioTek, VT Lab, USA) with an excitation wavelength of 450 nm and an emission wavelength of 490 nm.

2.11. Detection of Aβ structural species by Western blot

Aβ_{1-42} peptide film was dissolved in PBS to make a concentration of 20 μmol/L, which was incubated at 37 °C without or with the test drugs. After 24 h, 2 μL of each mixture was diluted with PBS and incubated with 0.01% glutaraldehyde (*v*/*v*) for 10 min. The crosslinking reaction was then terminated with 5.0 μL 5 × loading buffer containing 5% β-mercaptoethanol (Beyotime, Shanghai, China). All samples were subjected to sodium dodecyl sulfate-polyacrylamide gel (SDS-PAGE) electrophoresis without boiling. Subsequently, the peptide was transferred to polyvinylidene difluoride (PVDF) membranes (PALL, USA). After blocking with 5% milk in PBST, the membranes were incubated with the primary anti-Aβ monoclonal antibody 6E10 (1:2000, Biolegend) at 4 °C overnight. Then, the membranes were incubated with horseradish peroxidase (HRP)-linked secondary antibodies (1:2000) at room temperature for 1 h. Protein bands were detected by the UltraSignal™ ECL Substrate kit (4A Biotech Co., Ltd., Beijing, China) and visualized by BIO-RAD ChemiDoc™ Imaging System (Hercules, USA). Quantification of band intensity was performed using ImageJ software (National Institutes of Health, Bethesda, MD, USA).

2.12. Flow cytometry analysis

In addition to MTT assay, the viability of PC-12 cells was also evaluated by flow cytometry using the Annexin V-FITC/PE apoptosis detection kit (BD Biosciences, San Jose, CA, USA)[37]. Briefly, Aβ_{1-42}-induced PC-12 cells were treated with or without test drugs. After 24 h, cells were collected for centrifugation at a speed of 2000 rpm. The cell pellets were re-suspended and stained in 250 μL of 1 × Annexin V solution composed of 2 μL propidium iodide (PI) and 1 μL fluoresceine isothiocyanate (FITC) reagent in the dark for 15 min. Then, the analysis of cell death was performed on a flow cytometer (FACSverse, BD Biosciences, USA). Data analysis were performed with Flowjo 7.6.1 software (Tree Star, San Carlos, CA, USA).

2.13. Hoechst 33342/PI double staining assay

Moreover, cell death was also examined measured by the Hoechst 33342/PI staining method as described previously[38]. Briefly, Aβ_{1-42}-induced PC-12 cells on the coverslips were treated with or without test drugs. After 24 h, cells were subjected to fixation with 4% paraformaldehyde (PFA) reagent and PBS washing for 3 times, which was followed by a staining with 5 mg/L of Hoechst 33342 reagent and 5 mg/L of PI reagent. After incubation for 5 min, the representative images of cells at the same field were captured and merged by ImageXpress Micro4 (Molecular Devices, USA). Then, the death of PC-12 cells was measured by calculating the ratio of PI stained cells to the Hoechst 33342 stained cells.

2.14. C. elegans strains and maintenance conditions

The worm strains including N2 (wild type); CL4176, dvIs27 [*myo-3p*::A-Beta (1−42)::*let-851* 3′UTR) + *rol-6(su1006)*] X; CL2122, dvIs15 [(pPD30.38) *unc-54*(vector) + (pCL26) *mtl-2*::GFP]; CL2355, dvIs50 [pCL45 (*snb-1*::Abeta 1−42::3′ UTR(long) + *mtl-2*::GFP] I; and CL2331, dvIs37 [*myo-3p*::GFP::A-Beta (3−42) + *rol-6(su1006)*] were from Caenorhabditis Genetics Center (CGC, University of Minnesota, USA). All worms were cultured on plates covered with nematode growth media (NGM) and feed with *Escherichia coli* OP50 in an incubator at 20 °C unless otherwise noted.

2.15. Paralysis assay

The behavioral improvement effect of the test drugs *in vivo* was performed by measuring the paralysis ratio in the *C. elegans* models of AD[39]. In brief, CL4176 nematodes containing a heat-inducible human Aβ_{1-42} transgene expressed in muscle cells were transferred to NGM and treated with the test drugs. The temperature of incubator was shifted from 15 to 25 °C so as to stimulate Aβ expression and aggregation. After exposure to 25 °C for 36 h, the paralysis of worms was scored. The performance of nematodes which failed to move their bodies when touched or

exhibited a "halo" of cleared bacterial lawn while feeding was considered to be paralysis.

2.16. Food-searching behavior assay

CL2355 strains which express the human $A\beta_{1-42}$ and its vector control CL2122 strains were used to investigate the improvement effect of the test drugs on the food-sensing behavior. In brief, the plates were spread with *E. coli* OP50 in a ring with an outer diameter of 8 cm and an inner diameter of 1 cm[40]. After treatment with PPAC, DTA, TA, Cur or Poria extract for 48 h, worms were washed off and collected with M9 buffer and moved to an NGM agar plate which was pre-spotted with or without OP50 *E. coli* lawn. After 5 min, body-bends of worms were counted for 20 s intervals. The slowing of the body bending rate was calculated according to Eq.(3):

$$\text{Slowing rate} = \left(N_{\text{no food}} - N_{\text{food}}\right) / N_{\text{no food}} \quad (3)$$

where N indicates the numbers of body-bends of nematodes.

2.17. Preparation of worm proteins

After treatment, worms in the plates were collected into tubes with M9 buffer, which was followed by a centrifugation and washing to remove bacteria. The worms were then resuspended with 100 μL lysis buffer (50 mmol/L HEPES, 75 mmol/L sucrose, 1 mmol/L EDTA, 6 mmol/L $MgCl_2$, 1 mmol/L DTT, 25 mmol/L benzamidine, and 1% Triton X-100) in the presence of protease inhibitors. The lysis solution was sonicated for 3 times for 15 s on ice, which was followed by the centrifugation for 10 min at 14,000 rpm. Then, the supernatant was collected for the measurement of protein concentration using the Bio-RAD Bradford Protein Assay.

2.18. Detection of Aβ content in worms by dot blot analysis

Equal amount of worm protein was spotted on a 0.22 mm^2 PVDF membrane. Then, 5% nonfat milk was used to block the membrane for 1 h at room temperature. After wash with PBST, the membrane was incubated with the primary anti-Aβ monoclonal antibodies including 6E10, A11, and OC at 4 °C overnight. Then, the membrane was washed and subsequently incubated with the HRP-conjugated secondary antibody at room temperature. The antibody binding was detected using the UltraSignal™ ECL Substrate kit and visualized by a ChemiDoc™ Imaging System. Meanwhile, ponceau S (0.1%, *w/v*) solution (Saint-Bio, Shanghai, China) was used to stain the membrane for the visualization of total proteins.

2.19. Detection of Aβ content in worms by Western blot

Equal amount of worm protein in loading buffer (100 mmol/L DTT, 50 mmol/L Tris-HCl, pH 6.8, 10% glycerol, 5% SDS, 5% β-mercaptoethanol, and 0.02% bromophenol blue) was heated to 99 °C for 5 min. The electrophoresis was performed on a Tris-tricine SDS-PAGE using a constant voltage (150 V). Then, the proteins on gel were transferred to PVDF membranes. The membranes were blocked with 5% milk for 1 h at room temperature and followed by an overnight incubation with the primary anti-Aβ monoclonal antibody 6E10 (1:2000, Biolegend) at 4 °C overnight. Then, the membranes were incubated with the HRP-conjugated secondary antibody (1:2000) at room temperature for 1 h. After washing with TBST for 3 times, the membranes were detected by the UltraSignal™ ECL Substrate Kit and visualized by a BIO-RAD ChemiDoc™ Imaging System. Quantification of band was performed as described above.

2.20. $A\beta_{3-42}$ aggregation analysis

Aggregation of $A\beta_{3-42}$ was studied using CL2331 strains which temperature-sensitively express GFP bound to human $A\beta_{3-42}$ in body wall muscle[41]. Briefly, worms treated with PPAC, DTA, TA or Poria extract were incubated at 23 °C to induce $A\beta_{3-42}$ aggregation until day 2 of the adult worms. After treatment, the worms were mounted on glass slides containing 0.1% NaN_3. The representative images of worms were captured by a fluorescence microscope (Leica DM6B, Leica Microsystems GmbH, Germany). The total number of Aβ deposits in the anterior area was then calculated.

2.21. Molecular docking

Due to the lacking of crystal structure mono $A\beta_{1-42}$, a template-free modeling approach was used from a predicted distance/orientation matrix by deep residual neural networks training to the 3D model of human $A\beta_{1-42}$ in trRosetta, which used multiple sequence information from a multiple sequence alignment in the Protein Data Bank database. Following trRosetta, the inter-residue distance and orientation constraints minimization of 3D models of $A\beta_{1-42}$ was generated by neural network. Finally, the best fitted structure of $A\beta_{1-42}$ satisfying the restraints was selected as the initial model for further ligand-docking according to Rosetta energy score.

To further explore the interaction mechanism and the binding modes of PPAC, DTA, or TA with $A\beta_{1-42}$, a molecular docking study was performed using the DockThor protein−ligand docking program[42]. The SDF files of the ligands, including PPAC (CAS: 465-18-9), DTA (CAS: 6754-16-1), and TA (CAS: 508-24-7) were prepared from the NCBI Pubchem database. Then, the potential interaction modes between $A\beta_{1-42}$ and PPAC, DTA or TA were investigated, and the docked conformation was visualized by Pymol program.

2.22. Statistical analysis

All data were obtained from three or more independent experiments and presented as mean ± standard deviation (SD). One-way analysis of variance (ANOVA) followed by the post-Tukey test was conducted to analyze the significance of data using the GraphPad Prism 8.0 (San Diego, CA, USA). $P < 0.05$ was considered to have statistical significance among the compared groups.

3. Results

3.1. Screening of Aβ binding components in KXS

In our previous study, baicalin and baicalein were identified to be the potential inhibitors of Aβ fibrilization in SB by the UHPLC−DAD-Q/TOF-MS/MS analysis coupled with the pre-incubation of $A\beta_{1-42}$ with SB extract[31]. In this study, we established a novel HTS method for the screening of Aβ fibrilization inhibitors from natural medicines based on the combinational use of BLI and UHPLC−DAD-Q/TOF-MS/MS, and used SB to validate the feasibility of this method. After the dissociation of SB from the SA biosensor, the components in the dissociation buffer were then subjected to detection by UHPLC−DAD-Q/TOF-MS/MS, and the

RBA of the components in SB was determined. The curves indicating the association/dissociation binding of SB with Aβ and the kinetic constants suggested that the interaction of SB with Aβ was direct and reversible (Supporting Information Fig. S1A and Table S1). After dissociation of SB (400 μg/mL) from the biosensor for 5 times, the dissociation buffer with or without SB were collected and dried under the flow of nitrogen gas, respectively. At the same time, an equal volume of SB extract (400 μg/mL) used for the BLI assay was prepared in parallel. After analysis by the UHPLC−DAD-Q/TOF-MS/MS instrument. The representative total ion chromatograms (TICs) in Supporting Information Fig. S1B showed that some compounds in the dissociation buffer were detected when compared to SB extract alone. In addition, the Supporting Information Table S2 and Fig. S1C showed that baicalin and baicalein had the RBA in SB. Taken together, this method is a more effective, rapid, and reliable method for the screening of Aβ fibrillization inhibitor from natural medicines.

Table 1 The binding affinity (K_D), association rate constant (K_{on}) and dissociation rate constant (K_{dis}) of KXS to Aβ_{1-42}.

TCM	K_D (μg/mL)	K_{on} (L/mol·s)	K_{dis} (1/s)
KXS extract	170	1.15×10^2	2.6×10^{-2}

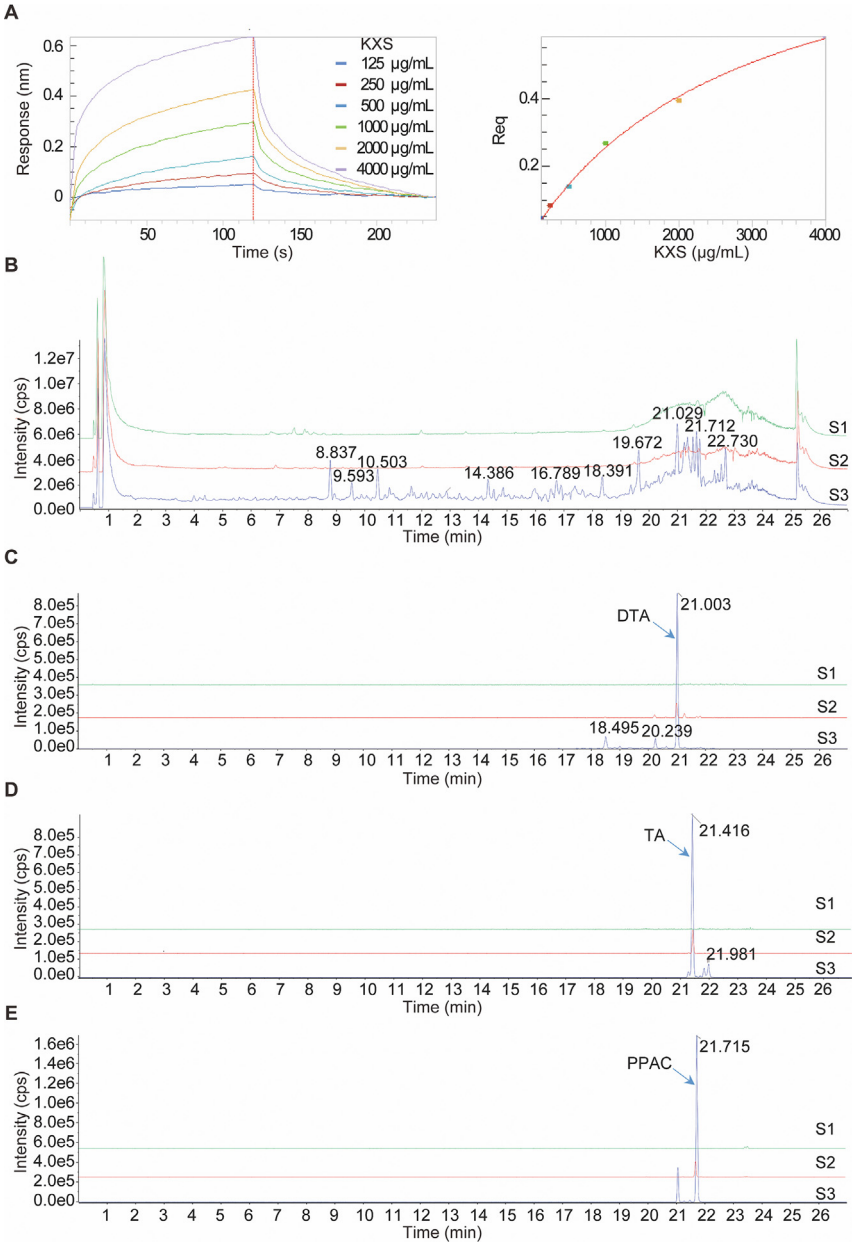

Figure 1 Screening of Aβ binding components in KXS by the combinational use of BLI and UHPLC−DAD-Q/TOF-MS/MS. (A) Real-time kinetic binding sensorgrams of different concentrations of KXS increasing from 125 to 4000 μg/mL are shown. Response (nm) indicates the optical thickness on the SA biosensor layer. The equilibrium binding signal (Req) revealed by the flattened curve is reached. (B) The TICs were recorded by UHPLC−DAD-Q/TOF-MS/MS. S1: The dissociation buffer without KXS extract; S2: The dissociation buffer with KXS extract; S3: KXS extract used for the BLI assay. (C) The extracted ion chromatograms (EICs) of dehydrotumulosic acid (DTA) in S1, S2, and S3. (D) The EICs of tumulosic acid (TA) in S1, S2, and S3. (E) The EICs of polyporenic acid C (PPAC) in S1, S2, and S3.

Table 2 The main detected components in KXS and their RBA (%) with Aβ.

Compd.	RT (min)	$[M-H]^-$ or $[M+HCOOH]^-$	Formula	MW	Chemcial name	RBA (%)
1	2.889	461.1143	$C_{19}H_{26}O_{13}$	462	Sibiricose A3	0.15
2	3.303	443.1772	$C_{20}H_{28}O_{11}$	444	Sibiricaphenone	0.04
3	3.409	431.1422	$C_{24}H_{32}O_7$	432	Acortatarinowin E	0.13
4	3.824	451.1092	$C_{21}H_{24}O_{11}$	452	Telephenone B	0.18
5	4.053	517.1389	$C_{22}H_{30}O_{14}$	518	Sibiricose A5	0.17
6	4.246	429.1259	$C_{19}H_{26}O_{11}$	430	Polygalatenoside B	0.11
7	4.44	547.1481	$C_{23}H_{32}O_{15}$	548	Sibiricose A6	0.18
8	5.435	547.1481	$C_{23}H_{32}O_{15}$	548	Sibiricose A1	0.12
9	6.229	537.1063	$C_{24}H_{26}O_{14}$	538	Sibiricaxanthone B	0.20
10	6.416	567.1163	$C_{25}H_{28}O_{15}$	568	Polygalaxanthone III	0.11
11	6.425	537.1063	$C_{24}H_{26}O_{14}$	538	Sibiricaxanthone A	0.11
12	6.531	607.1685	$C_{24}H_{34}O_{15}$	608	Sibiricose A2	0.14
13	6.773	567.1163	$C_{25}H_{28}O_{15}$	568	Polygalaxanthone VIII	0.19
14	6.963	567.1163	$C_{25}H_{28}O_{15}$	568	Polygalaxanthone XI	0.18
15	7.043	549.1429	$C_{26}H_{30}O_{13}$	550	Telephiose F	0.22
16	7.421	667.1659	$C_{30}H_{36}O_{17}$	668	Tenuifoliside B	0.12
17	7.638	607.1685	$C_{24}H_{34}O_{15}$	608	Dalmaisione D	0.11
18	7.676	753.1995	$C_{34}H_{42}O_{19}$	754	3′,4-Disinapoylsucrose	0.05
19	7.897	607.1685	$C_{24}H_{34}O_{15}$	608	Glomeratose A	0.05
20	8.098	521.185	$C_{24}H_{26}O_{13}$	522	Tricornoside C	0.11
21	8.34	521.185	$C_{24}H_{26}O_{13}$	522	Tricornoside F	0.10
22	8.839	753.1995	$C_{34}H_{42}O_{19}$	754	3,6′-Disinapoylsucrose	0.21
23	8.996	723.1903	$C_{33}H_{40}O_{18}$	724	3′-*O*-Feruloyl-6-*O* sinapoylsucrose	0.16
24	9.361	429.1264	$C_{19}H_{26}O_{11}$	430	Polygalatenoside C	0.00
25	9.601	681.1806	$C_{31}H_{38}O_{17}$	682	Tenuifoliside A	0.18
26	9.946	977.4995	$C_{47}H_{80}O_{18}$	933	Notoginsenoside R1	0.16
27	10.115	493.2122	$C_{25}H_{36}O_7$	448	Asarolignan D	0.12
28	10.507	845.4609	$C_{42}H_{72}O_{14}$	846	Ginsenoside Rg1	0.12
29	10.768	783.2088	$C_{42}H_{72}O_{13}$	784	Ginsenoside Rg2	0.10
30	10.92	767.2175	$C_{35}H_{44}O_{19}$	768	Tenuifoliside C	0.17
31	11.593	1307.3448	$C_{59}H_{72}O_{33}$	1308	Tenuifoliose I/J	0.05
32	11.674	1265.5381	$C_{57}H_{70}O_{32}$	1267	Tenuifoliose K	0.07
33	11.792	1337.353	$C_{60}H_{74}O_{34}$	1338	Tenuifoliose B	0.11
34	12.039	1235.529	$C_{65}H_{88}O_{23}$	1237	Arillatanoside A	0.03
35	12.237	1103.4905	$C_{53}H_{84}O_{24}$	1104	Polygalaxanthone XXVIII	0.12
36	12.242	1307.3448	$C_{59}H_{72}O_{33}$	1308	Tenuifoliose I/J	0.02
37	12.479	1337.353	$C_{60}H_{74}O_{34}$	1338	Tenuifoliose D	0.12
38	12.717	1349.3529	$C_{61}H_{74}O_{34}$	1350	Tenuifoliose H	0.09
39	12.928	1379.3626	$C_{62}H_{76}O_{35}$	1380	Tenuifoliose A	0.16
40	13.119	1409.3733	$C_{63}H_{78}O_{36}$	1410	Tenuifoliose N	0.00
41	13.38	1307.3448	$C_{61}H_{96}O_{30}$	1308	Polygalasaponin XXXIV	0.00
42	13.389	845.4609	$C_{42}H_{72}O_{14}$	846	Pseudoginsenoside F11	0.07
43	13.675	1337.353	$C_{60}H_{74}O_{34}$	1338	Senegose L	0.00
44	13.845	1307.3448	$C_{61}H_{96}O_{30}$	1308	Polygalasaponin XXXVII	0.00
45	13.93	815.4517	$C_{41}H_{70}O_{13}$	771	Notoginsenoside R2	0.05
46	14.387	1107.56	$C_{54}H_{92}O_{23}$	1109	Ginsenoside Rb1	0.05
47	14.586	1195.5702	$C_{56}H_{94}O_{24}$	1151	Quinquenoside R1	0.01
48	14.594	1193.5564	$C_{57}H_{94}O_{26}$	1195	Malonyl-ginsenoside Rb1	0.01
49	14.78	1077.5495	$C_{53}H_{90}O_{22}$	1079	Ginsenoside Rc	0.04
50	14.78	1123.5539	$C_{54}H_{92}O_{24}$	1125	Koryoginsenoside Rg2	0.03
51	14.908	955.4588	$C_{48}H_{76}O_{19}$	956	Ginsenoside Ro	0.21
52	14.994	1119.5584	$C_{55}H_{92}O_{23}$	1121	Ginsenoside Rs1	0.00
53	14.994	1163.5472	$C_{56}H_{92}O_{25}$	1165	Ginsenoside mRc	0.00
54	15.121	1077.5495	$C_{53}H_{90}O_{23}$	1079	Ginsenoside Rb2	0.03
55	15.121	1123.5539	$C_{54}H_{92}O_{24}$	1125	Notoginsenoside A	0.02
56	15.308	1119.5584	$C_{55}H_{92}O_{23}$	1121	Ginsenoside Rs2	0.00
57	15.308	1163.5472	$C_{56}H_{92}O_{25}$	1165	Ginsenoside mRb3	0.00
58	15.544	1617.6449	$C_{76}H_{114}O_{37}$	1619	Onjisaponin R	0.00
59	15.566	1195.5702	$C_{56}H_{94}O_{24}$	1151	Yesanchinoside F	0.00
60	15.773	1455.595	$C_{70}H_{104}O_{32}$	1457	Onjisaponin G	0.00
61	15.901	1761.6844	$C_{82}H_{122}O_{41}$	1763	Onjisaponin V	0.00
62	16.011	1119.5584	$C_{55}H_{92}O_{23}$	1121	Pseudoginsenoside F8	0.00
63	16.085	1485.606	$C_{71}H_{106}O_{33}$	1487	Onjisaponin E	0.10

(*continued on next page*)

Table 2 (*continued*)

Compd.	RT (min)	$[M-H]^-$ or $[M+HCOOH]^-$	Formula	MW	Chemcial name	RBA (%)
64	16.118	1659.6386	$C_{78}H_{116}O_{38}$	1661	Polygalasaponin XLV	0.00
65	16.237	1425.5885	$C_{69}H_{102}O_{31}$	1427	E-Senegasaponin B	0.00
66	16.329	1119.5584	$C_{55}H_{92}O_{23}$	1121	Pseudoginsenoside F8	0.00
67	16.334	1455.595	$C_{70}H_{104}O_{32}$	1457	Senegin II	0.00
68	16.343	1587.6325	$C_{75}H_{112}O_{36}$	1589	Polygalasaponin XXX	0.03
69	16.408	1703.6772	$C_{80}H_{120}O_{39}$	1705	Onjisaponin A	0.04
70	16.596	1847.7135	$C_{86}H_{128}O_{43}$	1849	Onjisaponin L	0.00
71	16.598	1587.6325	$C_{75}H_{112}O_{36}$	1589	Onjisaponin Wg	0.00
72	16.667	1599.6327	$C_{76}H_{112}O_{36}$	1601	Onjisaponin Gg	0.00
73	16.687	1731.6713	$C_{81}H_{120}O_{40}$	1733	Onjisaponin W	0.07
74	16.688	1631.6568	$C_{77}H_{116}O_{37}$	1633	Onjisaponin O	0.01
75	16.951	1617.643	$C_{76}H_{114}O_{37}$	1619	Polygalasaponin XLIV	0.03
76	16.995	1571.6369	$C_{75}H_{112}O_{35}$	1573	Onjisaponin B	0.01
77	17.112	1455.595	$C_{70}H_{104}O_{32}$	1457	*Z*-Senegin II	0.00
78	17.194	1541.6315	$C_{74}H_{110}O_{34}$	1543	Onjisaponin H	0.00
79	17.242	1761.6775	$C_{82}H_{122}O_{41}$	1763	Onjisaponin Vg	0.00
80	17.252	1673.6672	$C_{79}H_{118}O_{38}$	1675	Polygalasaponin XXXII	0.04
81	17.385	1469.61	$C_{71}H_{106}O_{32}$	1471	Onjisaponin Z	0.02
82	17.39	1659.6386	$C_{78}H_{116}O_{38}$	1661	Polygalasaponin XLVI	0.00
83	17.399	1685.6665	$C_{80}H_{118}O_{38}$	1687	Onjisaponin Ng	0.00
84	17.427	1425.5885	$C_{69}H_{102}O_{31}$	1427	Myrtifolioside C1	0.00
85	17.446	1817.7057	$C_{85}H_{126}O_{42}$	1819	Onjisaponin J	0.00
86	17.493	1791.691	$C_{83}H_{124}O_{42}$	1793	Onjisaponin T	0.00
87	17.677	1587.6325	$C_{75}H_{112}O_{36}$	1589	Onjisaponin F	0.01
88	17.691	1455.595	$C_{70}H_{104}O_{32}$	1457	Onjisaponin TH	0.00
89	17.743	1409.5909	$C_{69}H_{102}O_{30}$	1411	Onjisaponin Y	0.00
90	17.859	1425.5885	$C_{69}H_{102}O_{31}$	1427	*Z*-Senegasaponin B	0.07
91	17.995	1731.6713	$C_{81}H_{120}O_{40}$	1733	Onjisaponin Fg	0.01
92	18.007	1599.6327	$C_{76}H_{112}O_{36}$	1601	Onjisaponin K	0.00
93	18.391	499.3252	$C_{31}H_{48}O_5$	500	Poricoic acid GM	0.22
94	19.404	513.3043	$C_{31}H_{46}O_6$	514	Poricoic acid HM	0.23
95	19.681	497.3099	$C_{31}H_{46}O_5$	498	16α,25-Dihydroxydehydroeburi conic acid	0.26
96	21.003	483.2946	$C_{30}H_{44}O_5$	484	3-Epidehydrotumulosic acid	0.22
97	21.048	541.3348	$C_{33}H_{50}O_6$	542	6-Hydroxydehydropachymic acid	0.27
98	21.277	483.3306	$C_{30}H_{44}O_5$	484	Dehydrotumulosic acid	5.95
99	21.343	497.3099	$C_{31}H_{46}O_5$	498	Poricoic acid A	0.32
100	21.415	485.3461	$C_{31}H_{50}O_4$	486	Tumulosic acid	6.23
101	21.474	469.316	$C_{30}H_{46}O_4$	470	3β,16α-Dihydroxy-lanosta-7, 9(11),24-trien-21-oic acid	0.71
102	21.714	481.3159	$C_{31}H_{46}O_4$	482	Polyporenic acid C	2.23
103	22.317	511.3247	$C_{32}H_{48}O_5$	512	Poricoic acid AM	0.34
104	22.357	525.3395	$C_{33}H_{50}O_5$	526	Dehydropachymic acid	0.69
105	22.47	513.3407	$C_{31}H_{46}O_6$	514	3-*O*-Acetyl-16a-hydroxytrametenolic acid	0.31
107	22.585	525.3395	$C_{33}H_{50}O_5$	526	Poricoic acid AE	0.29
108	22.731	527.3554	$C_{33}H_{52}O_5$	528	Pachymic acid	0.26

Note: RT, retention time; MW, molecular weight; RBA, relative binding amount.

To further validate the feasibility of this newly developed screening method in more complex system, we employed it to screen the potential inhibitors of Aβ fibrillization from KXS, a classical formula widely used for the treatment of dementia, depression, and ageing. At first, the binding effect of KXS to Aβ_{1-42} was investigated by employing increasing concentrations of KXS extract (125, 250, 500, 1000, 2000, 4000 μg/mL) to monitor the real-time association/dissociation of KXS with biotinylated Aβ_{1-42}. The result showed that KXS had a direct and reversible interaction with Aβ_{1-42}, which was revealed by the concentration-dependent increase in response indicating the optical thickness (nm) on the sensor layer (Fig. 1A). In addition, the Table 1 showed that the kinetic constants including dissociation affinity (K_D) association rate (K_{on}), and dissociation rate constant (K_{dis}) calculated by the ForteBio data analysis software were 170 μg/mL, 1.15×10^2 L/mol•s, and 2.6×10^{-2} 1/s, respectively. Then, the dissociation solutions with or without KXS extract were collected for the UHPLC−DAD-Q/TOF-MS/MS analysis. After analysis of the representative TICs in Fig. 1B, the information including the retention time, accurate mass, molecular weight, chemical name, formula, and RBA of the detected components in KXS extract were obtained in Table 2. Among the binding components, three compounds in Poria, including polyporenic acid C (PPAC), dehydrotumulosic acid (DTA), and tumulosic acid (TA), showed the strongest binding affinity towards Aβ, which were demonstrated by the significant increased peak area and RBA in the dissociation buffer with KXS extract (Fig. 1C−E and Table 2). Collectively, the above data suggested that PPAC, DTA, and TA in Poria may be the main inhibitors of Aβ fibrillization that contribute to the neuroprotective effect of KXS in AD.

3.2. *Isolation and purification of PPAC, DTA, and TA from Poria*

Based on the above screening results, we aimed to isolate PPAC, DTA, and TA for the bioassay validation *in vitro* and *in vivo*. To begin, Poria crude powder were extracted with ethyl acetate reagent for three times using the reflux method. The dried extract was then subjected to separation by an open glass column filled with silica gel, and the components were eluted by the reagent system of methanol with dichloromethane. Then, the collected fractions were analyzed by UHPLC−DAD-Q/TOF-MS/MS and further purified by the pre-HPLC instrument. Finally, three compounds including PPAC, DTA, and TA were successfully isolated. The representative TIC of PPAC, DTA, TA, and Poria extract was acquired by UHPLC−DAD-Q/TOF-MS/MS instrument (Fig. 2A). The measured accurate mass of PPAC, DTA, and TA were $[M–H]^-$ 481.3388, $[M–H]^-$ 483.3510, and $[M–H]^-$ 485.3368, respectively (Fig. 2B), and their molecular structures were showed in Fig. 2C, which were consistent with the reported compounds[43].

3.3. *PPAC, DTA, and TA inhibit $A\beta_{1-42}$ fibrils formation*

To validate the feasibility and precision of this screening method, we firstly investigated the inhibitory effect of PPAC, DTA, and TA on the formation of $A\beta_{1-42}$ fibrils by ThT assay. Meanwhile, the extracts of Poria and KXS, and Cur were employed for comparison. It is well-known that the binding of ThT to $A\beta_{1-42}$ gives a relatively strong fluorescence signal at an emission wavelength of 482 nm which reflects the formation Aβ fibril[31]. At the time points of 0, 24, and 48 h, the fluorescence intensity of the solutions was detected by a spectrophotometer. As showed in Fig. 3A−C, $A\beta_{1-42}$ dramatically increased the ThT fluorescence, while the treatment of PPAC, DTA, TA, Cur, or the extract of Poria and KXS could decrease the intensity of fluorescence. Among these tested drugs, TA and Cur exhibited the best inhibitory effect on the formation Aβ fibrils. In addition, we detected the Aβ isoforms by Western blot using an anti-Aβ antibody (6E10). As shown in Fig. 3D, incubation with $A\beta_{1-42}$ alone led to the decreased level of both monomeric and oligomeric species. In the presence of PPAC, TA and Cur, monomeric (4 kDa), along with the dimeric, trimeric, tetrameric, and oligomeric (around 20 kDa) species were observed at the bottom of the gel. Therefore, the above results suggested that PPAC, TA and Cur inhibited Aβ fibrils formation and caused the accumulation of several intermediates including larger oligomeric to smaller monomer species. Taken together, PPAC, DTA, and TA can inhibit the formation of $A\beta_{1-42}$ fibrils.

3.4. *PPAC, DTA, and TA inhibit the cell death in $A\beta_{1-42}$-treated PC-12 cells*

Emerging evidence indicated that the extracellular Aβ fibril accumulates increasingly and induces cell death of neurons[44]. In current experiments, the improvement effect of PPAC, DTA, and

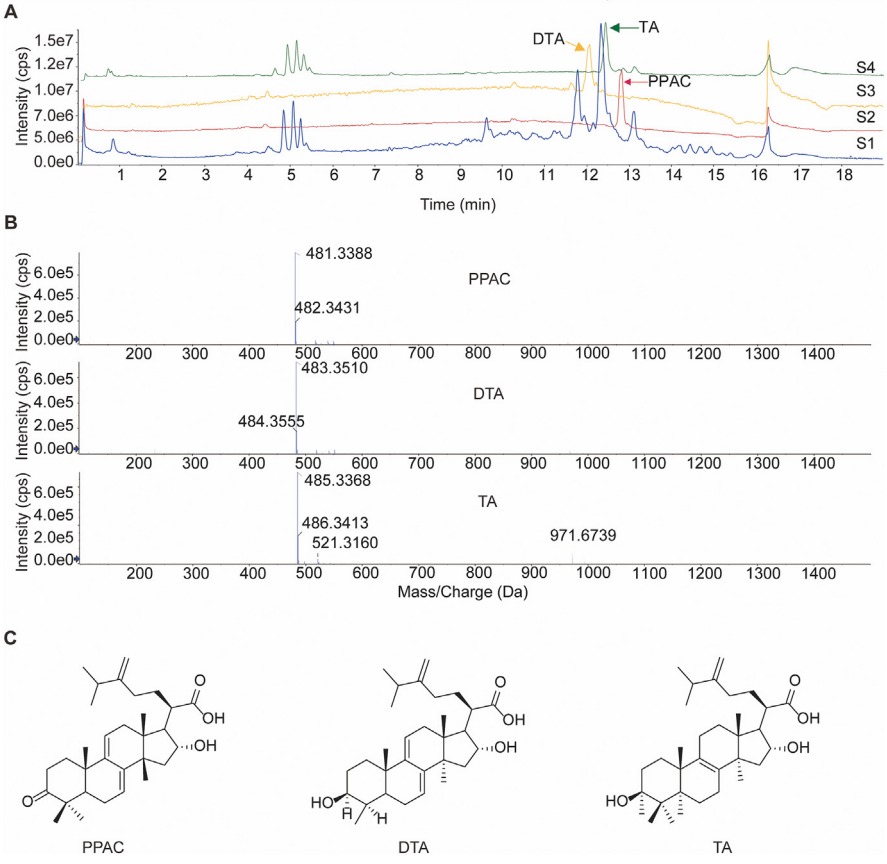

Figure 2 Isolation and purification of PPAC, DTA, and TA. (A) The TICs of PPAC, DTA, TA, and Poria extract. S1: Poria extract; S2: PPAC; S3: DTA; S4: TA. (B) The mass spectrums of PPAC, DTA, and TA. All the samples were analyzed by UHPLC−DAD-Q/TOF-MS/MS according to the chromatography condition in the method section. (C) The molecular structures of PPAC, DTA, and TA.

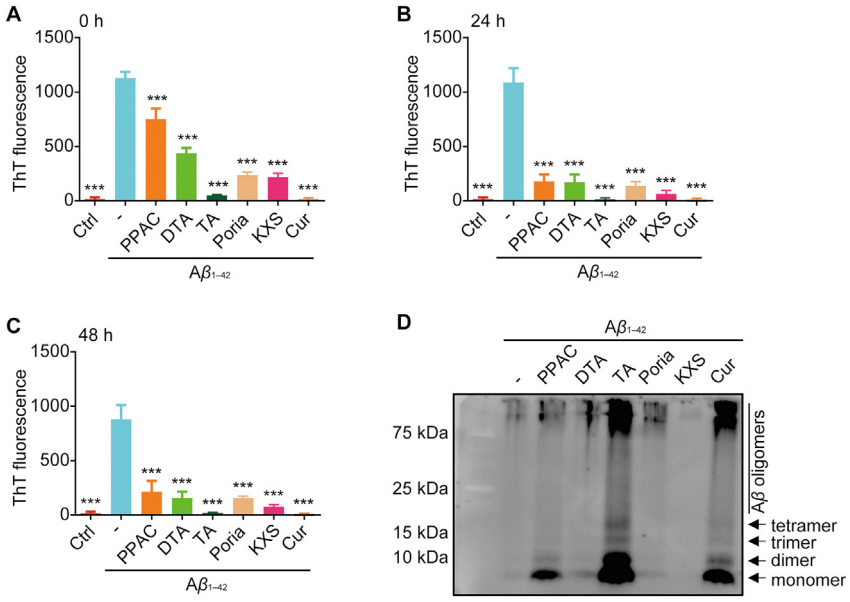

Figure 3 PPAC, DTA, and TA inhibit the formation of Aβ fibrils. 20 μmol/L $A\beta_{1-42}$ was incubated without or with Poria extract, KXS exctrat, PPAC, DTA, TA or Cur at 37 °C. At the time points of 0 h (A), 24 h (B), and 48 h (C), the solutions were mixed with 20 μmol/L of ThT solution. Then, the OD value of solutions was read by the spectrophotometer. The bar chart indicates the intensity of ThT fluorescence. (D) 20 μmol/L $A\beta_{1-42}$ peptide was incubated without or with Poria extract, KXS extract, PPAC, DTA, TA or Cur for 24 h. Then, the proteins were subjected to the crosslinking reaction and Western blot analysis using an anti-Aβ antibody (6E10). The arrows indicated Aβ monomer, dimer, trimer, tetramer, and oligomers. All data are representative of at least three independent experiments and are presented as mean ± SD, $n = 3$. ***$P < 0.001$. Poria extract: 20 μg/mL; KXS extract: 20 μg/mL; PPAC: 0.5 μmol/L; DTA: 0.5 μmol/L; TA: 0.5 μmol/L; Cur: 0.5 μmol/L.

TA on the cell viability of $A\beta_{1-42}$-induced PC-12 cells was investigated. At first, the cytotoxicity of PPAC, DTA, TA, Poria or KXS extract in PC-12 cells was measured by MTT method (Fig. 4A). Then, their effects on the cell viability were investigated in $A\beta_{1-42}$-treated PC-12 cells. As shown in Fig. 4B, PPAC, DTA, TA, Cur, and KXS extract significantly increased the cell viability of PC-12. Furthermore, by employing the flow cytometer and the Annexin V-FITC/PE apoptosis detection kit, we found that Poria extract, PPAC, DTA, TA, and Cur significantly decreased the cell death of $A\beta_{1-42}$-treated PC-12 cells (Fig. 4C). Moreover, the Hoechst/PI staining result indicated that Poria extract, PPAC, DTA, TA, and Cur could inhibit the cell death as revealed by the decreased percentage of cells with PI signal (Fig. 4D). Taken together, the above data indicated that PPAC, DTA, and TA inhibited the cells death of PC-12 induced by $A\beta_{1-42}$.

3.5. *PPAC, DTA, and TA improve the behavioral ability in C. elegans*

To investigate the neuroprotective effect of PPAC, DTA, and TA in the *in vivo* model of AD, *C. elegans*, a widely used model organism in neurodegenerative diseases, were used. As showed in Fig. 5A, Poria extract, and the single compounds including PPAC, DTA, TA, and Cur significantly decreased the percentage of worms of paralyzed in the transgenic *C. elegans* CL4176 strain, a nematode strain with temperature-induced expression of the human Aβ peptide in muscle cells. In addition, Aβ-induced *C. elegans* CL2355 and its control strain CL2122 were used for the study of the food-searching behavior. As shown in Fig. 5B, there were no significance difference observed among the control and treated groups in the CL2122 strain. However, the treatments of Poria extract, PPAC, DTA, TA, and Cur could significantly increase the slowing rate in the CL2355 strain. Taken together, the above data suggested that PPAC, DTA, and TA improved the behavioral function in the *C. elegans* models of AD.

3.6. *PPAC, DTA, and TA reduce Aβ species in C. elegans*

To determine if the effect of PPAC, DTA, and TA on delayed onset of paralysis was associated with a decrease in Aβ accumulation in transgenic CL4176, dot blot analysis was performed to detect the different isoforms of Aβ including prefibrillar oligomers (A11), fibrillary conformers (OC) and N terminus of Aβ (6E10) using different specific antibodies. As shown in Fig. 6A, PPAC, DTA, TA, Cur or Poria extract significantly decreased the expression of Aβ prefibrillar oligomers. Meanwhile, TA also dramatically decreased the level of Aβ fibrillar conformers and total Aβ. In addition, the Western blot analysis showed that the intensity of bands (9−20 kDa) representing Aβ oligomeric species was also reduced by PPAC, DTA, TA, Cur or Poria extract (Fig. 6B). Furthermore, we measured the Aβ deposits in the *C. elegans* CL2331 strain which temperature-sensitively expressed human $A\beta_{1-42}$ conjugated with GFP in the body wall muscle cells. As shown in Fig. 6C, Poria extract, PPAC, DTA, TA, and Cur significantly reduced the total number of Aβ deposits in the anterior area. Collectively, PPAC, DTA, and TA could inhibit Aβ accumulation both *in vitro* and *in vivo*.

3.7. *PPAC, DTA, and TA exhibit binding affinity towards $A\beta_{1-42}$*

The value of template modeling score of $A\beta_{1-42}$ model is 0.727 by the trRosetta[45], which identified that the confidence of the

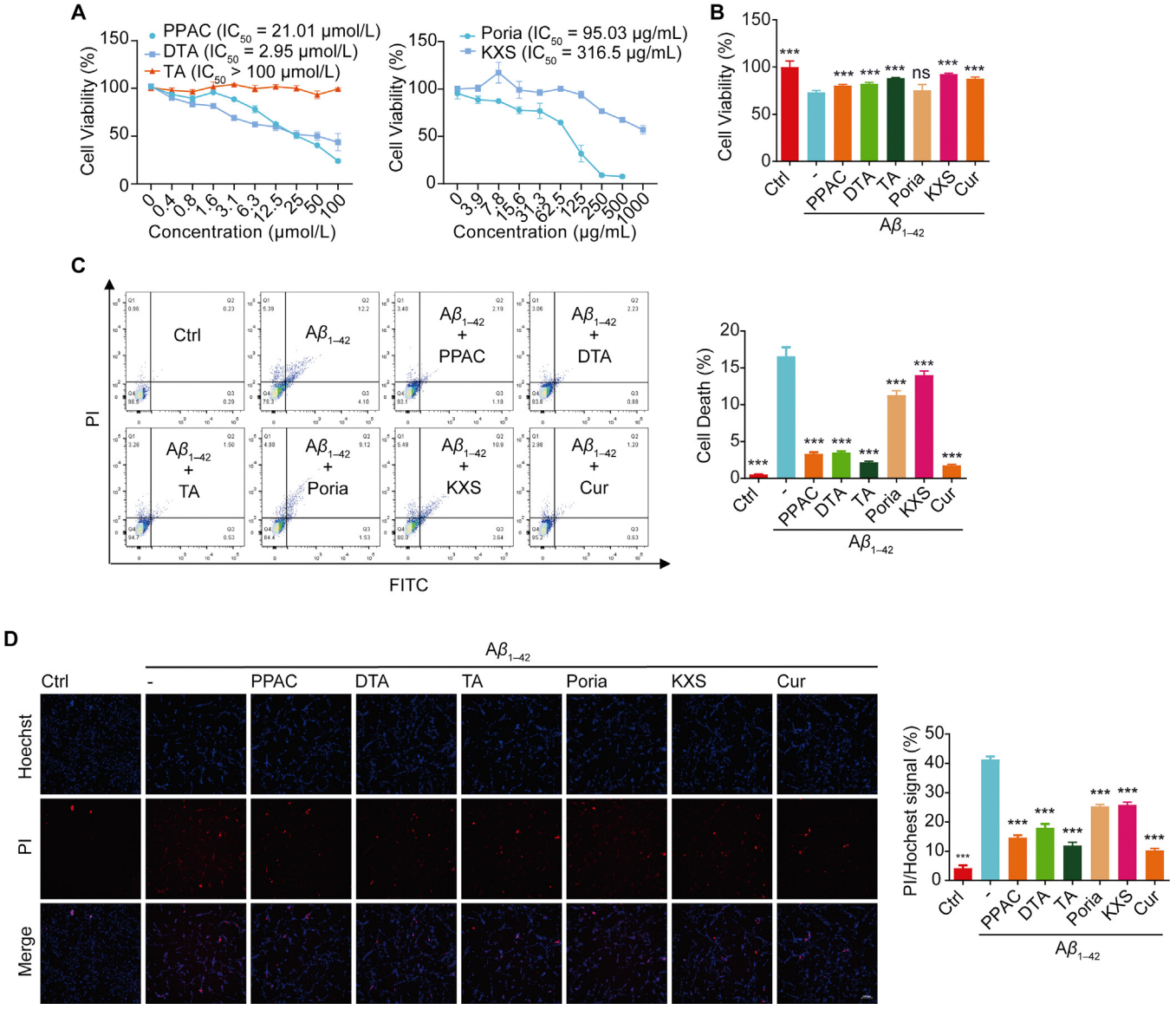

Figure 4 PPAC, DTA, and TA decrease the cytotoxicity in Aβ_{1-42}-induced PC-12 cells. (A) Cell viability of PC-12 cells treated with different concentrations of PPAC, DTA, TA, Poria or KXS extract at 24 h was examined using MTT assay. (B) PC-12 cells induced by Aβ_{1-42} were treated without or with PPAC, DTA, TA, Cur, Poria or KXS extract for 48 h. After treatment, the cell viability was measured by MTT assay. The bar chart indicates the viability of PC-12 cells. (C) PC-12 cells induced by Aβ_{1-42} were treated without or with PPAC, DTA, TA, Cur, Poria or KXS extract for 48 h. After treatment, cells were collected for the analysis of cell death by flow cytometer using a Annexin V-FITC/PE apoptosis kit. The bar chart represents the cell death of PC-12 cells. (D) PC-12 cells induced by Aβ_{1-42} were treated without or with PPAC, DTA, TA, Cur, Poria or KXS extract. After 48 h, cells were subjected to the staining with Hoechst33324/PI reagent for 5 min. The representative images were captured and merged at 10×magnification (Scale bar: 100 μm). The bar chart represents the ratio of PI/Hoechst signal of PC-12 cells. All data are representative of at least three independent experiment and are presented as mean ± SD, $n = 3$. ns: not significant, ***$P < 0.001$. Poria extract: 20 μg/mL; KXS extract: 20 μg/mL; PPAC: 0.5 μmol/L; DTA: 0.5 μmol/L; TA: 0.5 μmol/L; Cur: 0.5 μmol/L.

predicted model of Aβ_{1-42} is high. To identify a more desired binding site and the theoretical binding mode of PPAC, DTA, or TA on Aβ_{1-42} protein, we performed molecular docking-based calculations using DockThor service[46]. The docking-based calculations binding energy of PPAC, TA, and DTA on Aβ_{1-42} protein is −8.056, −7.656 and −7.359 kJ/mol (Fig. 7A and Table 3) as revealed by multiple solutions genetic algorithm, respectively. Besides, the total energy of PPAC, TA, and DTA on Aβ_{1-42} protein is 40.647, 43.795 and 43.053 kJ/mol as confirmed by MMFF94S force field methods. Therefore, PPAC, DTA, and TA were confirmed to have strong binding properties to Aβ. Based on the above *in vitro* and *in vivo* results, we further selected TA to validate its binding affinity with Aβ_{1-42} using BLI technology. As shown in Fig. 7B, TA exhibited a direct and reversible interaction with Aβ_{1-42} as revealed by the concentration-dependent increase in response indicating the optical thickness (nm) on the sensor layer. In addition, the kinetic constants including dissociation affinity (K_D), association rate (K_{on}), and dissociation rate (K_{dis}) were

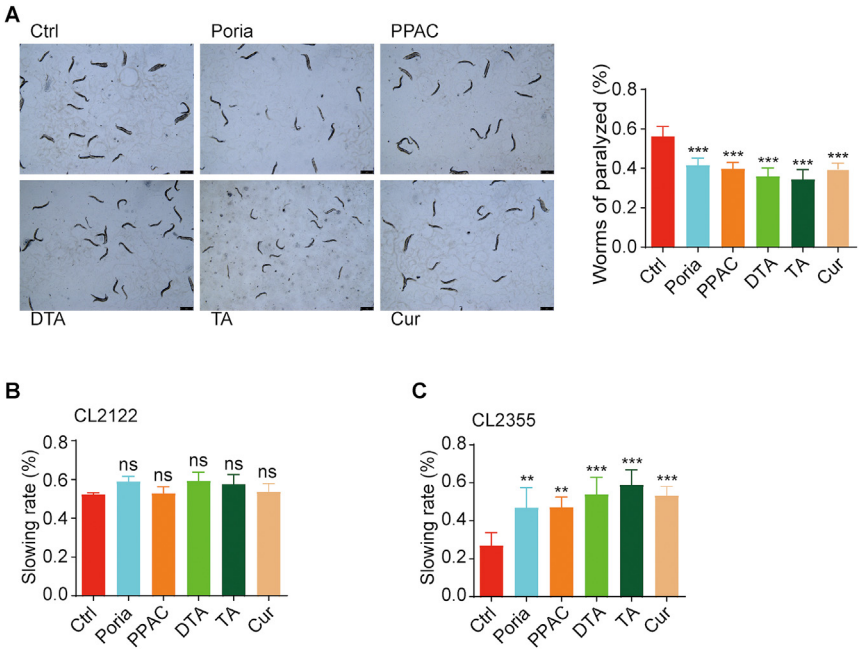

Figure 5 PPAC, DTA, and TA improve the behavioral function in *C. elegans*. (A) Aβ_{1-42}-induced CL4176 worms were treated without or with Poria extract, PPAC, DTA, TA or Cur for 72 h. After treatment, the representative images of worms were captured by a microscope at 10×magnification (Scale bars: 100 μm). The bar chart represents the quantification of worms ($n > 60$) that were not paralyzed. (B, C) Aβ-induced *C. elegans* CL2355 and its control strain CL2122 were treated with Poria extract, PPAC, DTA, TA or Cur for 72 h. After treatment, the food-sensing behavior was evaluated by counting the body bends of worms per 20 s on NGM plates in the absence or presence of food. The bar charts indicate the slowing rate of worms ($n = 20$). All data are representative of at least three independent experiment and are presented as mean ± SD. ns: not significant, $^{**}P < 0.01$, $^{***}P < 0.001$. Poria extract: 500 μg/mL; PPAC: 100 μmol/L; DTA: 100 μmol/L; TA: 100 μmol/L; Cur: 100 μmol/L.

49.9 μmol/L, 1.49 × 10^{+2} L/mol·s, and 7.42 × 10^{-3} 1/s, respectively (Table 4). Moreover, the UHPLC−DAD-Q/TOF-MS/MS analysis result indicated that TA could be detected in the dissociated solution (Fig. 7C). Collectively, PPAC, DTA, and TA exhibited the strongest binding affinity with Aβ among the screened compounds presented in KXS.

4. Discussion

AD is a progressive neurodegenerative disease with insidious onset. Clinically, the main symptoms are characterized by the memory impairment, executive dysfunction, impairment of visual spatial skills, personality and behavior changes[47]. In addition, AD is an age-related disease and has become the most common type of neurodegenerative disease, which increases exponentially with age and accounts for 60%−80% of all cases[48]. Emerging evidence indicates that accumulations of extracellular Aβ and hyperphosphorylation of intracellular Tau are recognized as two pathological characteristics of AD[5]. Among them, Aβ is mainly generated from amyloid precursor protein (APP) with the cleavage actions of β- and γ-secretase[49], and with the most common types as Aβ_{40} and Aβ_{42}. It is reported that Aβ aggregation can enhance the phosphorylation of Tau and facilitate tau seeding by promoting the internalization of the seeds[50]. In addition, the over-generation of Aβ produces a larger amount of reactive oxygen species (ROS), which results in neuronal death and microglial over-activation[51]. In addition, Aβ can promote the depolarization of the synaptic membrane, excessive influx of calcium and mitochondrial impairment. Moreover, there is a growing of evidence showing that amyloid deposition starts before the appearance of AD symptoms[52]. Therefore, the Aβ hypothesis is still prevailing in the mechanistic study of AD.

To date, although there are currently no drugs developed to cure AD, several prescription drugs are still approved by the US Food and Drug Administration (FDA) to alleviate the clinical symptoms of AD patients[53]. The clinical drugs mainly include the cholinesterase inhibitors (galantamine, rivastigmine, and donepezil) and *N*-methyl D-aspartate (NMDA) antagonists (namantine)[54]. However, there are still no drugs targeting Aβ or Tau approved to treat AD. Recently, most drugs for AD have failed due to its high difficulty of research and development and complexity of molecular mechanism. Therefore, most of the identified compounds are still in the stage of preclinical trial and discovery[55,56]. Of noted, FDA has just accepted the listing application of aducanumab, a monoclonal antibody targeting Aβ, based on the phase III clinical data on Alzheimer's early-stagy patients[57]. This application was recognized to be a landmark for new drugs. Therefore, targeting Aβ may be a promising strategy for the treatment of AD, and the discovery of Aβ aggregation inhibitors has become an important issue.

TCMs have a long history in the prevention and treatment of various diseases in China, which have been demonstrated to be safe and effective in the treatment of neurodegenerative diseases[58]. At present, EGb 761 (the extract of *Ginkgo biloba* L.) and huperzine A (an alkaloid of *Huperzia serrata*) have been widely used in clinical for the treatment of AD[59]. Although TCMs are the rich source of chemical compounds, the complexed components in

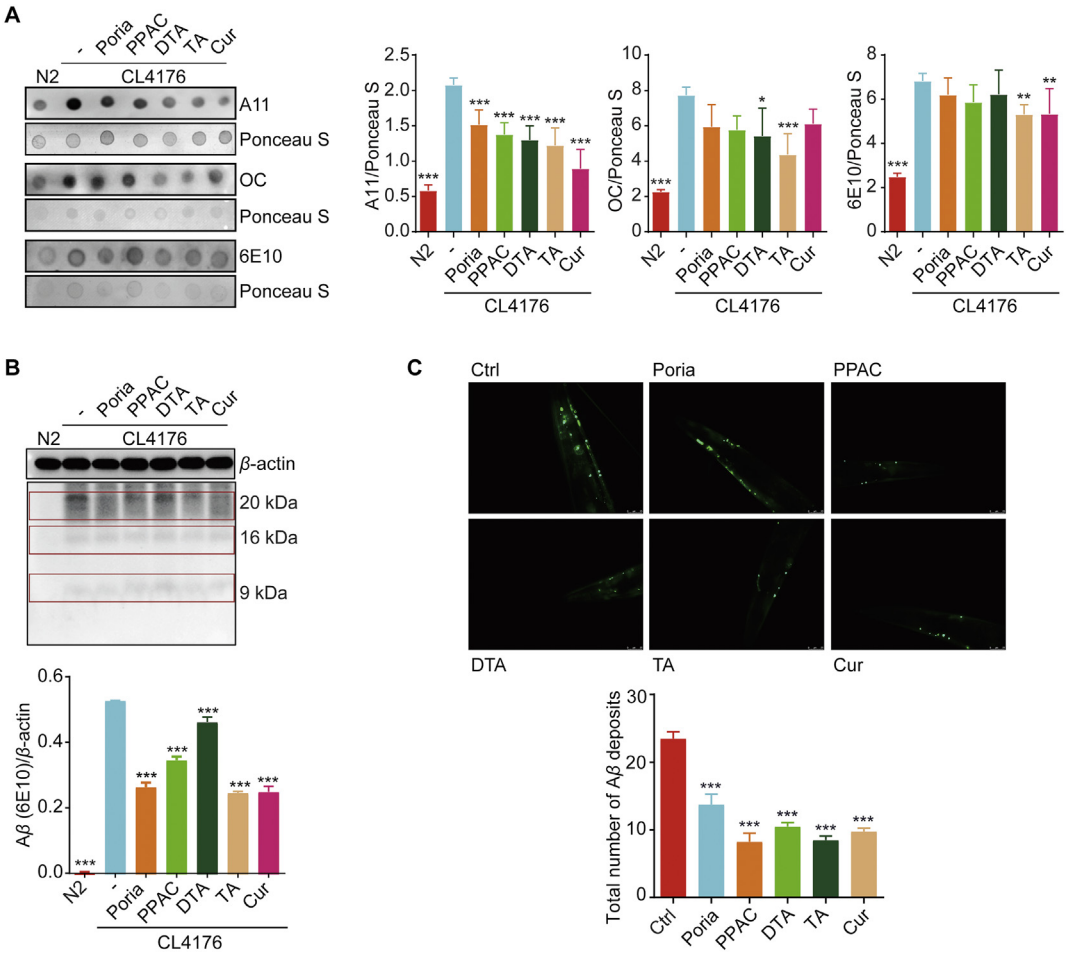

Figure 6 PPAC, DTA, and TA reduce Aβ species in *C. elegans*. (A) Synchronized L1 CL4176 worms were treated without or with Poria extract, PPAC, DTA, TA or Cur at 16 °C for 36 h, which was followed by an incubation for 36 h at 25 °C to induce the expression of Aβ. After treatment, worm proteins were collected for dot blot analysis of Aβ using antibodies including A11, OC, and 6E10 followed by Ponceau S staining. The bar chart indicates the ratio of A11/Ponceau S, OC/Ponceau S, and 6E10/Ponceau S in worms ($n \geq 1000$), respectively. N2: wild type worms. (B) After treatment, worm proteins were collected and subjected to the analysis of Aβ by Western blot using an anti-Aβ antibody (6E10). The bar chart indicates the ratio of Aβ oligomers/β-actin ($n \geq 1000$). N2: wild type worms. (C) CL2331 worms were treated with Poria extract, PPAC, DTA, TA or Cur for 72 h. After treatment, the representative images of the anterior area were captured using a fluorescence microscope at 40×magnification (scale bars: 25 μm). The bar chart indicates the total number of Aβ deposits in the anterior area of CL2331 worms ($n = 20$). All data are representative of at least three independent experiment and are presented as mean ± SD. ns: $^{*}P < 0.05$, $^{**}P < 0.01$, $^{***}P < 0.001$. Poria extract: 500 μg/mL; PPAC: 100 μmol/L; DTA: 100 μmol/L; TA: 100 μmol/L; Cur: 100 μmol/L.

a medical herb or even a Chinese medical formula hinder the process of the discovery of bioactive compounds. In general, the traditional bioactivity guided isolation and identification of the potential compounds from TCMs is time-consuming and laborious[24]. To date, there are many screening methods developed for the rapid discovery of bioactive compounds in the inhibition of Aβ based on the application of modern analytical instruments, including HPLC, MS, and NMR[29,30]. In our previous study, after incubation of the extract of *Polygonum cuspidatum* with methylglyoxal solution, two compounds, including polydatin and resveratrol, were identified as the natural methylglyoxal scavengers by UHPLC−DAD-MS hyphenated technique[31]. In addition, we employed cell membrane chromatography to identify 17 pentacyclic triterpenoid saponins from Radix Polygalae as the potent autophagy enhancers for the degradation of misfolded proteins associated with Parkinson's disease (PD) and Huntington's disease (HD). Moreover, we have recently developed a screening method to discover the Aβ inhibitors from SB based on the analysis of UHPLC−DAD-TOF/MS after the co-incubation of Aβ with SB extract. Through the comparison of the peak area between the solution with SB extract and the solution with SB and Aβ, we have successfully identified the compounds with decreased peak area as the Aβ inhibitors[31]. However, the physical adsorption of the components cannot be ruled out completely. Therefore, a more specific and reliable screening method for Aβ inhibitors is essential. BLI is a label-free technology for measuring the interaction of protein with protein or small molecule[60]. The target protein was first immobilized on the biosensor tips, then the small molecule or protein bound to the biosensor tip caused a shift that can be measured in real-time (Fig. 8). In this

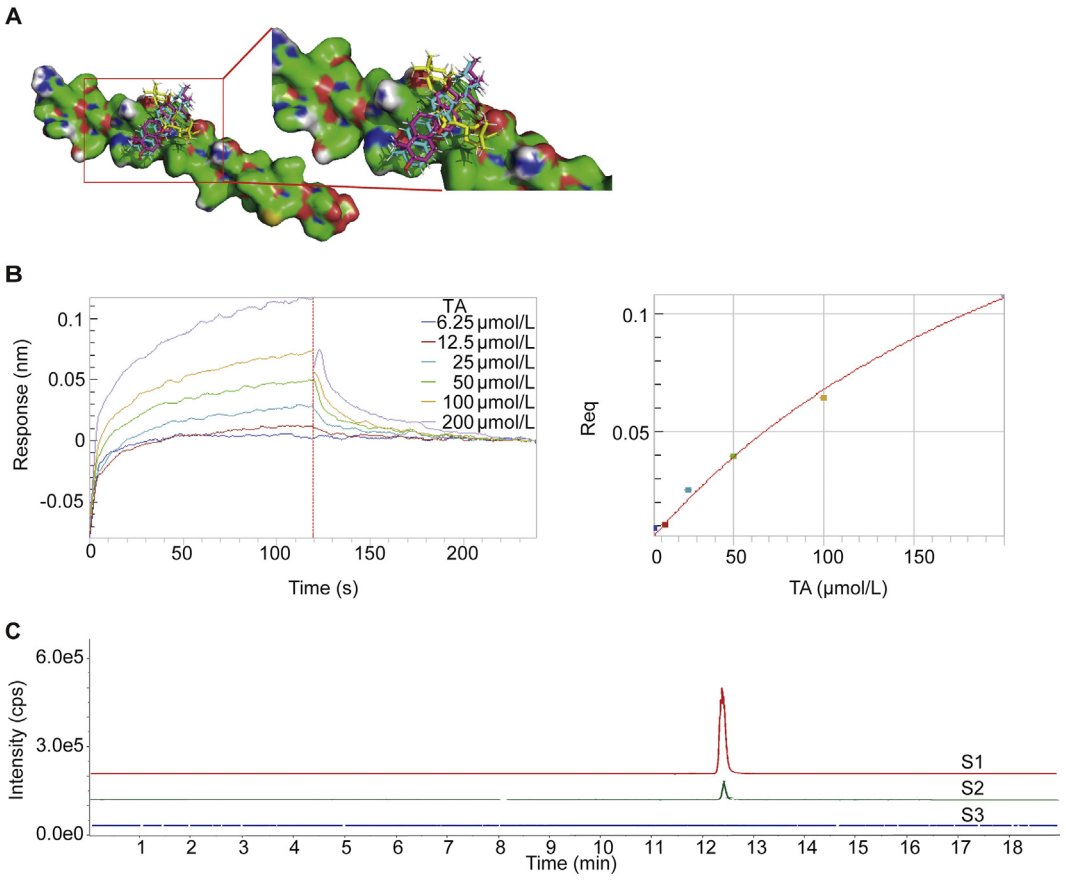

Figure 7 The binding of PPAC, DTA, and TA with Aβ_{1-42}. (A) Predicted binding modes of PPAC, TA and DTA against Aβ_{1-42} conformations. PPAC, TA and DTA are represented as cyan sticks, red sticks and yellow sticks, respectively. (B) Real-time kinetic binding sensorgrams of different concentrations of TA (12.5−400 μmol/L) are shown. Response (nm) indicates the optical thickness on the SA biosensor layer. The equilibrium binding signal (Req) revealed by the flattened curve is reached. (C) UHPLC–DAD-Q/TOF-MS/MS analysis of Mass spectrogram of TA: S1 represents TA, S2 represents the dissociated buffer, S3 represents the blank buffer.

Table 3 Molecular docking of PPAC, TA and DTA on Aβ_{1-42} using DockThor Server.

Chemical	Binding energy (kJ/mol)	Total energy (kJ/mol)
PPAC	−8.056	40.647
TA	−7.656	43.795
DTA	−7.359	43.053

study, we hypothesized that the components acting as Aβ inhibitors in the extract of TCMs could bind onto the biotinylated Aβ_{1-42}, while the components without biding property were washed away. Therefore, we used the ForteBio Octet® RED96e system to collect the components that were dissociated from the SA biosensor biotinylated with Aβ_{1-42}. Then, the components with binding affinity were collected and subjected to the UHPLC−DAD-Q/TOF-MS/MS analysis. Meanwhile, the dissociation buffer without natural medicine extract was set blank control, and the solution with natural medicine extract prepared for the BLI analysis was set reference for the detection of the components in natural medicines (Fig. 8). Finally, the RBA of the detected components in the dissociation solution were calculated, and the components with high RBA were proposed to be the potent inhibitors of Aβ fibrillization. In this study, SB was selected to validate the screening method, and we found that baicalein and baicalin were the potent Aβ inhibitors, which were consistent with our previous results[31]. KXS is an ancient Chinese medical formula that is composed of Radix Polygalae, Radix Ginseng, Poria, and Rhizoma Acori Tatarinowii. It is widely used to treat dementia and forgetfulness[33]. The modern pharmacological researches indicated that the KXS extract and its bioactive components exhibit potent neuroprotective effect in various cellular and animal models[61]. However, there are still no report on the systematic screening of Aβ inhibitors from KXS. In the present study, the potential Aβ inhibitors including DTA, TA, and PPAC were successfully screened out from KXS, which demonstrated that our currently developed screening method was high-throughput, feasible, and reliable. Moreover, both the *in vitro* and *in vivo* bioassays indicated that DTA, TA, and PPAC could inhibit Aβ fibrils formation, decrease the cytotoxicity of Aβ in PC-12 cells, and improve the behavioral abilities in *C. elegans*. In the future, this method will also be useful for the screening of the potential inhibitors from natural medicine that target other pathological proteins, such as Tau, α-synuclein, and huntingtin (HTT) associated with different neurodegenerative diseases.

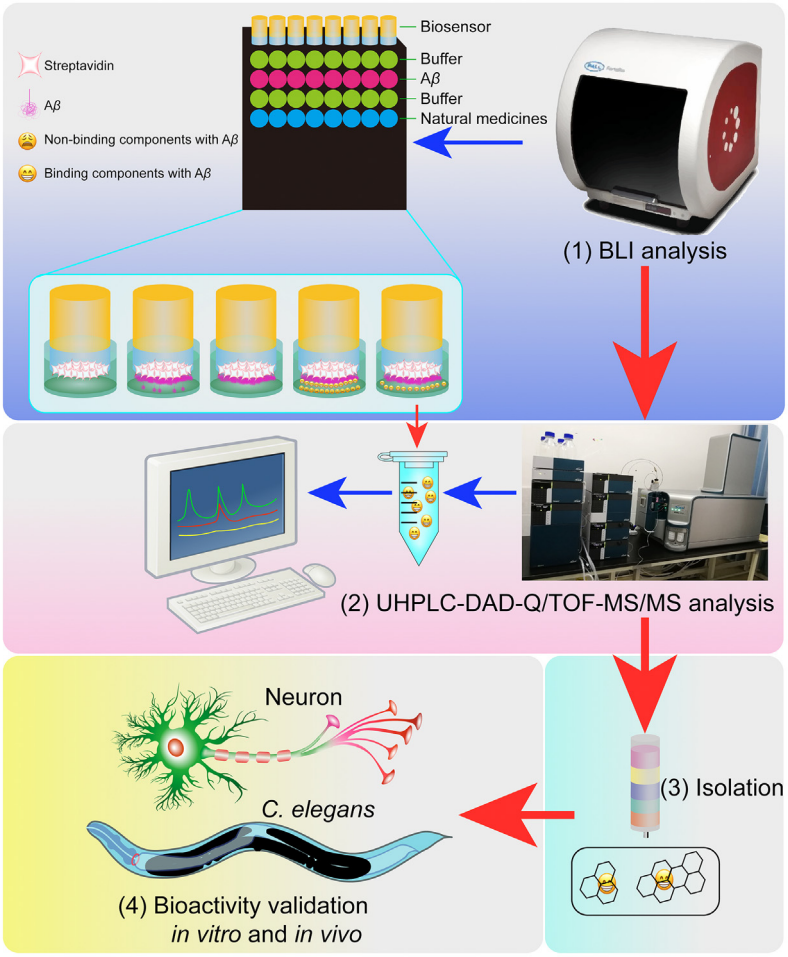

Figure 8 Schematic diagram of this HTS method and bioactivity validation of Aβ binding small molecules from natural medicines. (1) BLI analysis by Octet® RED96e system. (2) Identification by UHPLC−DAD-Q/TOF-MS/MS. (3) Isolation of the target ingredients from natural medicines. (4) Bioactivity validation of the screened Aβ binding small-molecules *in vitro* and *in vivo*.

Table 4 The binding affinity (K_D), association rate constant (K_{on}), and dissociation rate constant (K_{dis}) of TA to $A\beta_{1-42}$.

Compd.	K_D (μmol/L)	K_{on} (L/mol·s)	K_{dis} (1/s)
TA	49.9	$1.49 \times 10^{+2}$	7.42×10^{-3}

5. Conclusions

This study presents an effective, specific and reliable HTS method that is developed based on the combinational use of BLI and UHPLC−DAD-Q/TOF-MS/MS, which accelerates the discovery of natural small-molecule inhibitors of Aβ fibrils from natural medicines and the development of novel anti-AD drugs.

Acknowledgments

This work was supported by grants from the National Natural Science Foundation of China (81903829, 81801398). Department of Science and Technology of Sichuan Province, China (2018JY0474, 2019JDPT0010, 2021YJ0180, 21RCYJ0021, 202086, 2019YFSY0014). The Joint project of Luzhou Municipal People's Government and Southwest Medical University, China (2019LZXNYDJ02, 2019LZXNYDJ05, 2020LZXNYDJ37). The Science and Technology Planning Programs of Luzhou (2018-JYJ-34, China).

Author contributions

Anguo Wu, Xiaogang Zhou and Dalian Qin supervised the work. Anguo, Wu, Minsong Guo, Fengdan Zhu and Wenqiao Qiu performed all experiments. Min-Song Guo, Fengdan Zhu, Anguo Wu wrote the manuscript. Gan Qiao conducted the molecular docking. Yong Tang, Lu Yu and Jianming Wu provided the technical support. Chonglin Yu and Betty Yuen-Kwan Law helped with editing and English writing. Anguo Wu, Min-Song Guo, Fengdan Zhu and Betty Yuen-Kwan Law helped with manuscript revision and data collection.

Conflicts of interest

The authors declare no conflicts of interest.

Appendix A. Supporting information

Supporting information to this article can be found online at https://doi.org/10.1016/j.apsb.2021.08.030.

References

1. Tezel G, Timur SS, Bozkurt İ, Türkoğlu ÖF, Eroğlu İ, Nemutlu E, et al. A snapshot on the current status of Alzheimer's disease, treatment perspectives, *in-vitro* and *in-vivo* research studies and future opportunities. *Chem Pharm Bull (Tokyo)* 2019;**67**:1030−41.
2. Porteri C. Advance directives as a tool to respect patients' values and preferences: discussion on the case of Alzheimer's disease. *BMC Med Ethics* 2018;**19**:9.
3. Baumann B, Woehrer A, Ricken G, Augustin M, Mitter C, Pircher M, et al. Visualization of neuritic plaques in Alzheimer's disease by polarization-sensitive optical coherence microscopy. *Sci Rep* 2017;**7**:43477.
4. Kao YC, Ho PC, Tu YK, Jou IM, Tsai KJ. Lipids and Alzheimer's disease. *Int J Mol Sci* 2020;**21**:1505.
5. Grosso C, Valentão P, Ferreres F, Andrade PB. Bioactive marine drugs and marine biomaterials for brain diseases. *Mar Drugs* 2014;**12**:2539−89.
6. Richter M, Mewes A, Fritsch M, Krügel U, Hoffmann R, Singer D. Doubly phosphorylated peptide vaccines to protect transgenic P301S mice against Alzheimer's disease like tau aggregation. *Vaccines (Basel)* 2014;**2**:601−23.
7. Zaręba N, Kepinska M. The function of transthyretin complexes with metallothionein in Alzheimer's disease. *Int J Mol Sci* 2020;**21**:9003.
8. Mitroi DN, Karunakaran I, Gräler M, Saba JD, Ehninger D, Ledesma MD, et al. SGPL1 (sphingosine phosphate lyase 1) modulates neuronal autophagy *via* phosphatidylethanolamine production. *Autophagy* 2017;**13**:885−99.
9. Nury T, Lizard G, Vejux A. Lipids nutrients in Parkinson and Alzheimer's diseases: cell death and cytoprotection. *Int J Mol Sci* 2020;**21**:2501.
10. Chen S, Chen ST, Sun Y, Xu Z, Wang Y, Yao SY, et al. Fibroblast growth factor 21 ameliorates neurodegeneration in rat and cellular models of Alzheimer's disease. *Redox Biol* 2019;**22**:101133.
11. Wu S, Tan G, Dong X, Zhu Z, Li W, Lou Z, et al. Metabolic profiling provides a system understanding of hypothyroidism in rats and its application. *PLoS One* 2013;**8**:e55599.
12. Mohamad Zobir SZ, Mohd Fauzi F, Liggi S, Drakakis G, Fu X, Fan TP, et al. Global mapping of traditional Chinese medicine into bioactivity space and pathways annotation improves mechanistic understanding and discovers relationships between therapeutic action (Sub)classes. *Evid Based Compl Alternat Med* 2016;**2016**:2106465.
13. Jiménez-Aliaga K, Bermejo-Bescós P, Benedí J, Martín-Aragón S. Quercetin and rutin exhibit antiamyloidogenic and fibril-disaggregating effects *in vitro* and potent antioxidant activity in APPswe cells. *Life Sci* 2011;**89**:939−45.
14. Jiang W, Luo T, Li S, Zhou Y, Shen XY, He F, et al. Quercetin protects against okadaic acid-induced injury *via* MAPK and PI3K/Akt/GSK3β signaling pathways in HT22 hippocampal neurons. *PLoS One* 2016;**11**:e0152371.
15. Dong YT, Cao K, Tan LC, Wang XL, Qi XL, Xiao Y, et al. Stimulation of SIRT1 attenuates the level of oxidative stress in the brains of APP/PS1 double transgenic mice and in primary neurons exposed to oligomers of the amyloid-β peptide. *J Alzheimers Dis* 2018;**63**:283−301.
16. Xiong R, Zhou XG, Tang Y, Wu JM, Sun YS, Teng JF, et al. Lychee seed polyphenol protects the blood–brain barrier through inhibiting Aβ(25-35)-induced NLRP3 inflammasome activation *via* the AMPK/mTOR/ULK1-mediated autophagy in bEnd.3 cells and APP/PS1 mice. *Phytother Res* 2021;**35**:954−73.
17. Qiu WQ, Pan R, Tang Y, Zhou XG, Wu JM, Yu L, et al. Lychee seed polyphenol inhibits Aβ-induced activation of NLRP3 inflammasome via the LRP1/AMPK mediated autophagy induction. *Biomed Pharmacother* 2020;**130**:110575.
18. Keowkase R, Kijmankongkul N, Sangtian W, Poomborplab S, Santaardharnpreecha C, Weerapreeyakul N, et al. Protective effect and mechanism of fruit extract of *Aegle marmelos* against amyloid-β toxicity in a transgenic *Caenorhabditis elegans*. *Nat Prod Commun* 2020;**15**:1−12.
19. Tang Y, Yu C, Wu J, Chen H, Zeng Y, Wang X, et al. Lychee seed extract protects against neuronal injury and improves cognitive function in rats with type II diabetes mellitus with cognitive impairment. *Int J Mol Med* 2018;**41**:251−63.
20. Kim MJ, Kim JH, Kim JH, Lee S, Cho EJ. Amelioration effects of *Cirsium japonicum* var. maackii extract/fractions on amyloid beta25-35-induced neurotoxicity in SHSY5Y cells and identification of the main bioactive compound. *Food Funct* 2020;**11**:9651−61.
21. Cui L, Zhang Y, Cao H, Wang Y, Teng T, Ma G, et al. Ferulic acid inhibits the transition of amyloid-β42 monomers to oligomers but accelerates the transition from oligomers to fibrils. *J Alzheimers Dis* 2013;**37**:19−28.
22. tefănescu BE, Szabo K, Mocan A, Crişan G. Phenolic compounds from five Ericaceae species leaves and their related bioavailability and health benefits. *Molecules* 2019;**24**:2046.
23. Ye M, Moon J, Yang J, Lim HH, Hong SB, Shim I, et al. The standardized Lycium chinense fruit extract protects against Alzheimer's disease in 3xTg-AD mice. *J Ethnopharmacol* 2015;**172**:85−90.
24. Yuan XY, Wang M, Lei S, Yang QX, Liu YQ. Rapid screening of active components with an osteoclastic inhibitory effect in herba epimedii using quantitative pattern-activity relationships based on joint-action models. *Molecules* 2017;**22**:1767.
25. Yan X, Wang S, Yu A, Shen X, Zheng H, Wang L. Cell chromatography-based screening of the active components in buyang huanwu decoction promoting axonal regeneration. *BioMed Res Int* 2019;**2019**:6970198.
26. Gu L, Hong F, Fan K, Zhao L, Zhang C, Yu B, et al. Integrated network pharmacology analysis and pharmacological evaluation to explore the active components and mechanism of *Abelmoschus manihot* (L.) Medik. on renal fibrosis. *Drug Des Dev Ther* 2020;**14**:4053−67.
27. Tao Y, Chen Z, Zhang Y, Wang Y, Cheng Y. Immobilized magnetic beads based multi-target affinity selection coupled with high performance liquid chromatography-mass spectrometry for screening antidiabetic compounds from a Chinese medicine "Tang-Zhi-Qing". *J Pharmaceut Biomed Anal* 2013;**78−79**:190−201.
28. Gu X, Wang D, Wang X, Liu Y, Di X. Fast screening of biomembrane-permeable compounds in herbal medicines using bubble-generating magnetic liposomes coupled with LC-MS. *Molecules* 2021;**26**:1742.
29. Zhang M, Liu Y, Liu M, Liu B, Li N, Dong X, et al. UHPLC–QTOF/MS-based metabolomics investigation for the protective mechanism of Danshen in Alzheimer's disease cell model induced by A$\beta_{1\text{-}42}$. *Metabolomics* 2019;**15**:13.
30. Ciaramelli C, Palmioli A, De Luigi A, Colombo L, Sala G, Salmona M, et al. NMR-based *Lavado cocoa* chemical characterization and comparison with fermented cocoa varieties: insights on cocoa's anti-amyloidogenic activity. *Food Chem* 2021;**341**:128249.
31. Yu L, Wu AG, Wong VK, Qu LQ, Zhang N, Qin DL, et al. The new application of UHPLC–DAD-TOF/MS in identification of inhibitors on β-amyloid fibrillation from *Scutellaria baicalensis*. *Front Pharmacol* 2019;**10**:194.
32. Zhang SQ, Obregon D, Ehrhart J, Deng J, Tian J, Hou H, et al. Baicalein reduces β-amyloid and promotes nonamyloidogenic amyloid precursor protein processing in an Alzheimer's disease transgenic mouse model. *J Neurosci Res* 2013;**91**:1239−46.
33. Zhu Y, Duan X, Cheng X, Cheng X, Li X, Zhang L, et al. Kai-Xin-San, a standardized traditional Chinese medicine formula, upregulates the expressions of synaptic proteins on hippocampus of chronic mild stress induced depressive rats and primary cultured rat hippocampal neuron. *J Ethnopharmacol* 2016;**193**:423−32.
34. Heller GT, Aprile FA, Michaels TCT, Limbocker R, Perni M, Ruggeri FS, et al. Small molecule sequestration of amyloid-β as a drug discovery strategy for Alzheimer's disease. *Sci Adv* 2020;**6**:eabb594.
35. Klein AN, Ziehm T, Tusche M, Buitenhuis J, Bartnik D, Boeddrich A, et al. Optimization of the all-D peptide D3 for abeta oligomer elimination. *PLoS One* 2016;**11**:e0153035.

36. Lu J, Cao Q, Wang C, Zheng J, Luo F, Xie J, et al. Structure-based peptide inhibitor design of amyloid-β aggregation. *Front Mol Neurosci* 2019;**12**:54.
37. Zhang L, Yang Y, Di L, Li JL, Li N. Erxian decoction, a famous Chinese medicine formula, antagonizes corticosterone-induced injury in PC12 cells, and improves depression-like behaviours in mice. *Pharm Biol* 2020;**58**:498−509.
38. Sun YB, Zhao H, Mu DL, Zhang W, Cui J, Wu L, et al. Dexmedetomidine inhibits astrocyte pyroptosis and subsequently protects the brain in *in vitro* and *in vivo* models of sepsis. *Cell Death Dis* 2019;**10**:167.
39. Saraceno C, Musardo S, Marcello E, Pelucchi S, Di Luca M. Modeling Alzheimer's disease: from past to future. *Front Pharmacol* 2013;**4**:77.
40. Mohankumar A, Shanmugam G, Kalaiselvi D, Levenson C, Nivitha S, Thiruppathi G, et al. East indian sandalwood (*Santalum album* L.) oil confers neuroprotection and geroprotection in *Caenorhabditis elegans via* activating SKN-1/Nrf2 signaling pathway. *RSC Adv* 2018;**8**: 33753−74.
41. Aprile FA, Sormanni P, Podpolny M, Chhangur S, Needham LM, Ruggeri FS, et al. Rational design of a conformation-specific antibody for the quantification of Aβ oligomers. *Proc Natl Acad Sci U S A* 2020;**117**:13509−18.
42. Sankaranarayanan NV, Bi Y, Kuberan B, Desai UR. Combinatorial virtual library screening analysis of antithrombin binding oligosaccharide motif generation by heparan sulfate 3-*O*-sulfotransferase 1. *Comput Struct Biotechnol J* 2020;**18**:933−41.
43. Zhu LX, Xu J, Wang RJ, Li HX, Tan YZ, Chen HB, et al. Correlation between quality and geographical origins of *Poria cocos* revealed by qualitative fingerprint profiling and quantitative determination of triterpenoid acids. *Molecules* 2018;**23**:2200.
44. Söllvander S, Nikitidou E, Gallasch L, Zyśk M, Söderberg L, Sehlin D, et al. The Aβ protofibril selective antibody mAb158 prevents accumulation of Aβ in astrocytes and rescues neurons from Aβ-induced cell death. *J Neuroinflammation* 2018;**15**:98.
45. Yang J, Anishchenko I, Park H, Peng Z, Ovchinnikov S, Baker D. Improved protein structure prediction using predicted interresidue orientations. *Proc Natl Acad Sci U S A* 2020;**117**:1496−503.
46. Santos KB, Guedes IA, Karl ALM, Dardenne LE. Highly flexible ligand docking: benchmarking of the DockThor program on the LEADS-PEP protein-peptide data set. *J Chem Inf Model* 2020;**60**:667−83.
47. Xu F, Na L, Li Y, Chen L. Roles of the PI3K/AKT/mTOR signalling pathways in neurodegenerative diseases and tumours. *Cell Biosci* 2020;**10**:54.
48. Al Rihani SB, Darakjian LI, Kaddoumi A. Oleocanthal-rich extra-virgin olive oil restores the blood–brain barrier function through NLRP3 inflammasome inhibition simultaneously with autophagy induction in TgSwDI mice. *ACS Chem Neurosci* 2019;**10**:3543−54.
49. Chen GF, Xu TH, Yan Y, Zhou YR, Jiang Y, Melcher K, et al. Amyloid beta: structure, biology and structure-based therapeutic development. *Acta Pharmacol Sin* 2017;**38**:1205−35.
50. Shin WS, Di J, Cao Q, Li B, Seidler PM, Murray KA, et al. Amyloid β-protein oligomers promote the uptake of tau fibril seeds potentiating intracellular tau aggregation. *Alzheimer's Res Ther* 2019;**11**:86.
51. Chen HJ, Shen YC, Shiao YJ, Liou KT, Hsu WH, Hsieh PH, et al. Multiplex brain proteomic analysis revealed the molecular therapeutic effects of buyang huanwu decoction on cerebral ischemic stroke mice. *PLoS One* 2015;**10**:e0140823.
52. Bodart-Santos V, de Carvalho LRP, de Godoy MA, Batista AF, Saraiva LM, Lima LG, et al. Extracellular vesicles derived from human Wharton's jelly mesenchymal stem cells protect hippocampal neurons from oxidative stress and synapse damage induced by amyloid-β oligomers. *Stem Cell Res Ther* 2019;**10**:332.
53. Iranshahy M, Javadi B. Diet therapy for the treatment of Alzheimer's disease in view of traditional Persian medicine: a review. *Iran J Basic Med Sci* 2019;**22**:1102−17.
54. Walker VM, Davies NM, Kehoe PG, Martin RM. What is the impact of regulatory guidance and expiry of drug patents on dementia drug prescriptions in England? A trend analysis in the Clinical Practice Research Datalink. *Alzheimer's Res Ther* 2018;**10**:51.
55. Mancuso C, Gaetani S. Preclinical and clinical issues in Alzheimer's disease drug research and development. *Front Pharmacol* 2014;**5**:234.
56. Colligris P, Perez de Lara MJ, Colligris B, Pintor J. Ocular Manifestations of Alzheimer's and other neurodegenerative diseases: the sprospect of the eye as a tool for the early diagnosis of Alzheimer's disease. *J Ophthalmol* 2018;**2018**:8538573.
57. Sanchez L, Richter J, Cho HJ, Jagannath S, Madduri D, Parekh S, et al. Subcutaneous daratumumab and hyaluronidase-fihj in newly diagnosed or relapsed/refractory multiple myeloma. *Ther Adv Hematol* 2021;**12**:1−12.
58. Chang XH, Liang LN, Zhan LB, Lu XG, Shi X, Qi X, et al. The effect of Chinese Jinzhida recipe on the hippocampus in a rat model of diabetes-associated cognitive decline. *BMC Compl Alternative Med* 2013;**13**:161.
59. Howes MR, Fang R, Houghton PJ. Effect of Chinese herbal medicine on Alzheimer's disease. *Int Rev Neurobiol* 2017;**135**:29−56.
60. Rosen O, Ozeri E, Barnea A, David AB, Zichel R. Development of an innovative *in vitro* potency assay for anti-botulinum antitoxins. *Toxins (Basel)* 2016;**8**:276.
61. Guo S, Wang J, Xu H, Rong W, Gao C, Yuan Z, et al. Classic prescription, Kai-Xin-San, ameliorates Alzheimer's disease as an effective multitarget treatment: from neurotransmitter to protein signaling pathway. *Oxid Med Cell Longev* 2019;**2019**:9096409.